Small, R.G. (1968) Coats' disease and muscular dystrophy. *Trans. Am. Acad. Ophthal. Otolaryng.* 72: 225–231.

Takeya, T., Hamano, K., Kawashima, K., Iwasaki, N., Ohhashi, T., Sato, T. (1990) [Facioscapulohumeral muscular dystrophy (FSH) and hearing loss]. *No To Hattatsu* 22: 24–29.

Tawil, R., McDermott, M.P., Mendell, J.R., Kissel, J., Griggs, R.C. (1994) Facioscapulohumeral muscular dystrophy (FSHD): design of natural history study and results of baseline testing. FSH-DY Group. *Neurology* 44: 442–446.

Taylor, D., Carroll, J., Smith, M., Johnson, M., Johnston, G., Brooke, M. (1982) Facioscapulohumeral dystrophy associated with hearing loss and Coats syndrome. *Ann. Neurol.* 12: 395–398.

Tonini, M., Passos-Bueno, M., Cerqueira, A., Pavanello, R., Vainzof, M., Dubowitz, V., Zatz, M. (2002) Facioscapulohumeral (FSHD1) and other forms of muscular dystrophy in the same family: is there more in muscular dystrophy than meets the eye? *Neuromusc. Disord.* 12: 554–557.

van der Kooi, A.J., Visser, M.C., Rosenberg, N., van den Berg-Vos, R., Wokke, J.H., Bakker, E., de Visser, M. (2000) Extension of the clinical range of facioscapulohumeral dystrophy: report of six cases. *J. Neurol. Neurosurg. Psych.* 69: 114–116.

Verhagen, W.I., Huygen, P.L., Padberg, G.W. (1995) The auditory, vestibular, and oculomotor system in facioscapulohumeral dystrophy. *Acta Otolaryngol. Suppl.* 520: 140–142.

Voit, T., Lamprecht, A., Lenard, H.G., Goebel, H.H. (1986) Hearing loss in facioscapulohumeral dystrophy. *Eur. J. Pediatr.* 145: 280–285.

Yamamoto, S., Matsushima, H., Kawai, N., Sotobata, I. (1986) [Myocardial involvement in muscular dystrophy evaluated by thallium-201 emission computed tomography]. *J. Cardiogr.* 16: 373–385.

Yamanaka, G., Goto, K., Matsumura, T., Funakoshi, M., Komori, T., Hayashi, Y. K., Arahata, K. (2001) Tongue atrophy in facioscapulohumeral muscular dystrophy. *Neurology* 57: 733–735.

Yamanaka, G., Goto, K., Hayashi, Y. K., Miyajima, T., Hoshika, A., Arahata, K. (2002) [Clinical and genetical features of Japanese early-onset facioscapulohumeral muscular dystrophy]. *No To Hattatsu* 34: 318–324.

Yasukohchi, S., Yagi, Y., Akabane, T., Terauchi, A., Tamagawa, K., Mizuno, Y. (1988) Facioscapulohumeral dystrophy associated with sensorineural hearing loss, tortuosity of retinal arterioles, and an early onset and rapid progression of respiratory failure. *Brain Dev.* 10: 319–324.

Available online at www.sciencedirect.com
SCIENCE DIRECT®
Biochemical and Biophysical Research Communications 320 (2004) 639–647
BBRC
www.elsevier.com/locate/ybbrc

Reduction of insulin-stimulated glucose uptake by peroxynitrite is concurrent with tyrosine nitration of insulin receptor substrate-1☆

Takashi Nomiyama,[a] Yasuhiro Igarashi,[a] Hikari Taka,[b] Reiko Mineki,[b] Toyoyoshi Uchida,[a] Takeshi Ogihara,[a] Jong Bock Choi,[a] Hiroshi Uchino,[a] Yasushi Tanaka,[a] Hiroshi Maegawa,[c] Atsunori Kashiwagi,[c] Kimie Murayama,[b] Ryuzo Kawamori,[a] and Hirotaka Watada[a,*]

[a] *Department of Medicine, Metabolism and Endocrinology, Juntendo University, School of Medicine, Tokyo, Japan*
[b] *Central Laboratory of Medical Sciences, Juntendo University, School of Medicine, Tokyo, Japan*
[c] *Division of Endocrinology and Metabolism, Department of Medicine, Shiga University of Medical Science, Otsu, Japan*

Received 8 May 2004

Abstract

Inducible nitric oxide synthetase plays an essential role in insulin resistance induced by a high-fat diet. The reaction of nitric oxide with superoxide leads to the formation of peroxynitrite ($ONOO^-$), which can modify several proteins. In this study, we investigated whether peroxynitrite impairs insulin-signalling pathway. Our experiments showed that 3-(4-morpholinyl)sydnonimine hydrochloride (SIN-1), a constitutive producer of peroxynitrite, dose-dependently inhibited insulin-stimulated glucose uptake. While SIN-1 did not affect the insulin receptor protein level and tyrosine phosphorylation, it reduced the insulin receptor substrate-1 (IRS-1) protein level, and IRS-1 associated phosphatidylinositol-3 kinase (PI-3 kinase) activity. Although SIN-1 did not induce Ser^{307} phosphorylation of IRS-1, tyrosine nitration of IRS-1 was detected in SIN-1-treated-Rat1 fibroblasts expressing human insulin receptors. Mass spectrometry showed that peroxynitrite induced at least four nitrated tyrosine residues in rat IRS-1, including Tyr^{939}, which is critical for association of IRS-1 with the p85 subunit of PI-3 kinase. Our results suggest that peroxynitrite reduces the IRS-1 protein level and decreases phosphorylation of IRS-1 concurrent with nitration of its tyrosine residues.

Keywords: Insulin resistance; Oxidative stress; Insulin receptor substrate-1; Nitric oxide; iNOS; Peroxynitrite

Nitric oxide (NO) has many physiological functions in the central nervous system, cardiovascular system, and immune system, acting as a signal transduction molecule to control diverse biological functions such as vasodilatation [1] and the secretion of neurotransmitters [2]. On the other hand, excessive NO production is involved in inflammation, and thus plays an important role in the pathophysiology of various diseases. Among the three isoforms of nitric oxide synthetase (NOS), inducible NOS (iNOS) is known to produce far larger amounts of NO compared with the other isoforms, and iNOS has been recognized to play a role in the pathogenesis of inflammatory and autoimmune diseases, such as septic shock, hemorrhagic shock, rheumatoid arthritis, osteoarthritis, inflammatory bowel disease, and

☆ *Abbreviations:* BSA, bovine serum albumin; CBB, Coomassie brilliant blue R250; Da, Dalton; DMEM, Dulbecco's modified Eagle's medium; DTT, dithiothreitol; EDTA, ethylenediaminetetraacetic acid; Erk, extracellular signalling-regulated kinase; FCS, fetal calf serum; HIRc, rat-1 fibroblasts expressing human insulin receptors; iNOS, inducible NOS; IRS, insulin receptor substrate; LC, liquid chromatography; MAPK, mitogen-activated protein kinase; MS, mass spectrometry; NO, nitric oxide; *NONOate*, (*Z*)-1-{*N*-[3-aminopropyl]-*N*-[4-(3-aminopropylammonio)butyl]-amino}-diazen-1-ium-1,2-diolate; NOS, nitric oxide synthetase; NP-40, Nonidet P-40; PAGE, polyacrylamide gel electrophoresis; PBS, phosphate-buffered saline; PDA, polydiacetylene; PI3-kinase, phosphatidylinositol-3 kinase; PMSF, phenylmethylsulphonyl fluoride; SIN-1, 3-(4-morpholinyl)sydnonimine hydrochloride; TFA, trifluoroacetic acid; *TNF; tumour necrosis* factor.

* Corresponding author. Fax: +81-3-3813-5996.
E-mail address: hwatada@med.juntendo.ac.jp (H. Watada).

0006-291X/$ - see front matter © 2004 Elsevier Inc. All rights reserved.
doi:10.1016/j.bbrc.2004.06.019

multiple sclerosis [3,4]. NO can also be viewed as a radical containing an unpaired electron. In addition to reacting with superoxide (O_2^-), NO is transformed into peroxynitrite ($ONOO^-$) [5], which is a highly reactive radical.

Peroxynitrite can modify tyrosine residues and form nitrotyrosine in various proteins. Nitration of protein tyrosine residues can lead to damage that alters protein function and stability [6]. It also often affects signal transduction pathways by disrupting tyrosine phosphorylation [7,8], because tyrosine phosphorylation is commonly involved in signal transduction. For example, the insulin signal transduction pathway involves the tyrosine phosphorylation of several proteins, so peroxynitrite might impair the action of insulin through nitration of key tyrosine residues on the proteins involved in insulin signalling.

Tumour necrosis factor-α (TNF-α) causes insulin resistance in obese subjects and probably promotes the expression of iNOS [9]. Recently, Perreault and Marette [10] found that targeted disruption of iNOS was almost completely protective against high-fat diet-induced insulin resistance in mice. This finding suggests that activation of iNOS per se plays a key role in high-fat diet-induced insulin resistance in vivo although its mechanism has not yet been fully elucidated.

The present study was designed to investigate whether peroxynitrite induced insulin resistance. Our results indicated that peroxynitrite could impair insulin-stimulated glucose uptake by 3T3-L1 adipocytes. Analysis of the insulin signal transduction pathway revealed marked repression of insulin receptor substrate-1 (IRS-1)-associated phosphatidylinositol-3 (PI3)-kinase activity after exposure to peroxynitrite. These changes were concurrent with a reduction of the IRS-1 protein level and tyrosine phosphorylation of this protein. In addition, mass spectrometric analysis (MS) revealed that exposure of rat IRS-1 to peroxynitrite provoked the nitration of at least four tyrosine residues including Tyr^{939}, which is one of the critical docking sites of the p85 subunit of PI3-kinase.

Materials and methods

Antibodies and reagents. Human insulin was purchased from Wako Chemicals (Tokyo, Japan). Anti-nitrotyrosine antibody, anti-IRS-1 antibody, anti-p85 antibody, anti-serine (307)-phosphorylated IRS-1 antibody, and rat recombinant IRS-1 were obtained from Upstate Biotechnology Incorporated (Lake Placid, NY). Anti-phosphotyrosine (PY69), anti-insulin receptor β subunit antibody, and anti-Akt1/2 antibody were from Santa Cruz Biotechnology (Santa Cruz, CA). Anti-threonine (308), serine (473) phosphospecific Akt antibody, and anti-phosphospecific extracellular signalling-regulated kinase (Erk) antibody were from Cell Signaling Technology (Beverly, MA). TNF-α was purchased from R&D Systems (Minneapolis, MN). Horseradish peroxidase-conjugated anti-rabbit and anti-mouse antibodies were purchased from Bio-Rad Laboratories (Tokyo). 3-(4-Morpholinyl)sydnonimine hydrochloride (SIN-1) and peroxynitrite were obtained from Dojin Tech. (Kumamoto, Japan). (*Z*)-1-{*N*-[3-Aminopropyl]-*N*-[4-(3-aminopropylammonio)butyl]-amino}-diazen-1-ium-1, 2-diolate (spermine NONOate) was purchased from Alexis Biochemicals (Tokyo).

Cell culture. Preadipocyte-derived 3T3-L1 cells (purchased from ATCC) were cultured in high-glucose Dulbecco's modified Eagle's medium (DMEM) supplemented with 10% fetal calf serum (FCS). To induce differentiation into adipocytes, the cells were incubated with isobutylmethylxanthine (500 μM), dexamethazone (25 μM), and insulin (4 μg/ml) for 3 days and then with insulin alone for another 3 days until more than 95% cells had differentiated. Then the cells were trypsinized and reseeded in appropriate culture dishes for further experiments [11].

Rat1 fibroblasts expressing human insulin receptors (HIRc) provided by Dr. J.M. Olefsky were grown and maintained in low-glucose DMEM (Invitrogen, San Diego, CA) containing 50 U/ml streptomycin and 10% FCS under a 10% CO_2 environment.

2-Deoxyglucose uptake. Glucose uptake was measured by the methods of Klip et al. [12] with minor modifications. 3T3-L1 adipocytes were incubated with or without SIN-1, spermine NONOate or MnTBAP for 12 h in high-glucose DMEM with 2% FCS, followed by incubation in glucose-free DMEM supplemented with 0.2% bovine serum albumin (BSA) in the absence or presence of 100 nM insulin for 1 h at 37 °C. After the addition of 10 μl of 2-[^{3}H]deoxyglucose or L-[^{3}H]deoxyglucose (0.1 μCi), the cells were incubated for 5 min and glucose uptake was determined from the 2-[^{3}H]deoxyglucose counts in each cell lysate. To obtain a concentration at which cell membrane transport was rate-limited, the value for L-glucose was subtracted to correct each sample for the contributions of diffusion and trapping. The data were corrected by the protein concentrations measured by the method of Bradford, as described previously [13].

Immunoprecipitation assay and Western blotting. 3T3-L1 adipocytes and HIRc cells were serum-starved for 12 h in a medium with or without 4 or 8 mM SIN-1. Then the cells were stimulated with 100 nM insulin for 5 or 20 min at 37 °C. After washing three times with ice-cold phosphate-buffered saline (PBS), the cells were lysed in lysis buffer (20 mM Tris–HCl [pH 7.5], 1 mM ethylenediaminetetraacetic acid [EDTA], 140 mM NaCl, 1% Nonidet P-40 [NP-40], 1 mM Na_3VO_4, 1 mM phenylmethylsulphonyl fluoride [PMSF], 50 mM NaF, and 10 μl/ml proteinase cocktail [Sigma, St. Louis, MO]). Cellular lysates were obtained after sonication and centrifugation. For the immunoprecipitation assay, lysates containing 1 mg of total protein were incubated with the indicated antibodies for 12 h at 4 °C. Especially, to elucidate the effect of SIN-1 on insulin signalling directly associated with IRS-1, we used half dose of anti-IRS-1 antibody as recommended by the manufacturer to obtain a similar amount of IRS-1 protein from each sample. After collection on protein A or G Sepharose, the immune complexes were washed three times with 1 ml lysis buffer, and Western blotting analysis was performed as described previously [13].

PI3-kinase assay. 3T3-L1 adipocytes were serum-starved for 16 h in the presence or absence of 4 mM SIN-1. Then the cells were incubated in the presence or absence of 100 nM insulin for 20 min. After washing twice with ice-cold washing buffer (20 mM Tris–HCl [pH 7.5], 1 mM $MgCl_2$, 1 mM $CaCl_2$, 137 mM NaCl, and 100 μM Na_3VO_4), the cells were lysed with lysis buffer (washing buffer plus 10% glycerol, 1% NP-40, 1 mM PMSF, and 10 μl/ml proteinase cocktail). After sonication and centrifugation, the supernatant (containing 1.5 mg protein) was incubated with anti-IRS-1 antibody for 2 h and then incubated with protein A–Sepharose for 12 h at 4 °C. The resulting immunoprecipitates were washed three times with PBS containing 1% NP-40, 100 μM Na_3VO_4, three times with 100 mM Tris–HCl (pH 7.5), 500 mM LiCl, and 100 μM Na_3VO_4, and twice with 10 mM Tris–HCl (pH 7.5), 100 mM NaCl, 1 mM EDTA, and 100 μM Na_3VO_4. Pellets were suspended in 50 μl of 10 mM Tris–HCl (pH 7.5), 100 mM NaCl, 1 mM EDTA, and 100 μM Na_3VO_4. The reaction was initiated by the addition of 200 μM ATP, 1.11 MBq [γ-^{32}P]ATP, 10 mM $MgCl_2$, and 10 μg

phosphatidylinositol. Incubation was performed at 30 °C for 10 min and the reaction was terminated with the addition of 8 N HCl. After extraction with $CHCl_3$ and CH_3OH (1:1), the aqueous phase was applied to a silica gel thin-layer chromatography plate. The plate was developed in $CHCl_3$:CH_3OH:H_2O:NH_4OH (100:70:15:25), dried, visualized, and quantified with a BAS2500 (Fuji film, Tokyo).

Separation of recombinant IRS-1 by 1-dimensional SDS–polyacrylamide gel electrophoresis. The gel for separation of IRS-1 was prepared as described previously [14]. The electrophoresis apparatus was a product of Nihon Eido (Tokyo) and a gel size measuring 130 × 130 × 1 mm was used for 1-dimensional SDS–polyacrylamide gel electrophoresis (SDS–PAGE) (12 lanes). The concentrations of polyacrylamide in the separating and stacking gels were 6% and 3%, respectively, while that of polydiacetylene (PDA) as a cross-linker was 2.6%/acrylamide. One milligram of rat recombinant IRS-1 (Upstate Biotechnology) was incubated in PBS with or without 50 μM peroxynitrite for 1 h at 4 °C. For immunoprecipitation, the samples were incubated with 4 μg anti-IRS-1 antibody and collected on protein A–Sepharose. For in-gel digestion, immunoprecipitates were washed three times with PBS and boiled with modified Laemmli sample buffer (62.5 mM Tris–HCl [pH 8.5], containing 10% glycerol, 2% SDS, 0.1 M dithiothreitol [DTT], and 0.0025% bromophenol blue). After cooling at room temperature, 5 μl aliquots of 30% acrylamide stock solution were added for in situ alkylation of the cysteinyl residues of proteins. Immediately after mixing, the samples were loaded onto a stacking gel. SDS–PAGE was commenced at 5 mA for 1 h in order to concentrate the proteins in the stacking gel and then the proteins were separated at 10 mA per gel for 2 h. The running buffer consisted of 25 mM Tris and 19.2 mM glycine (pH 8.45) containing 0.1% SDS, according to Laemmli [15].

In-gel trypsin digestion of IRS-1. After completing SDS–PAGE, proteins were visualized by staining with Coomassie brilliant blue R250 (CBB). The approximately 150 kilodalton (kDa) band was excised with a razor blade and cut into small pieces, which were placed in an Eppendorf tube, and washed with 50% acetonitrile and 100 mM ammonium bicarbonate in purified water for 10 min at 37 °C. Then the gel pieces were dehydrated by addition of acetonitrile for 10 min at 37 °C and dried in a vacuum centrifuge (Micro Vac MV-100; Tomy, Tokyo). The dried samples were immersed in 30–50 μl trypsin at 10 ng/μl, dissolved in 100 mM ammonium bicarbonate (pH 8.5), and let to stand for 15–18 h at 37 °C. The trypsinized peptides were extracted with the following solutions (50 μl of each) for 10 min at 37 °C: (i) 50% acetonitrile containing 0.1% trifluoroacetic acid (TFA), (ii) a mixture of isopropanol:formic acid:acetonitrile:purified water (15:20:25:40 v/v), and (iii) 80% acetonitrile. Extracts were evaporated to dryness in a vacuum centrifuge and used to identify IRS-1 by MS.

Identification of IRS-1 and its nitrated tyrosine residues by MS. Peptide mapping was carried out using the APIQSTAR Pulsar hybrid mass spectrometer system (Foster City, CA) with a micro liquid chromatograph (LC) (Magic 2002; Michrom BioResource, Auburn, CA). The conditions for micro LC were as follows: a Magic C18 column (0.2 mm ID × 50 mm) was eluted with 0.1% formic acid in solvent A, and 0.1% formic acid in 90% acetonitrile (solvent B) using the following program; 5% solvent B for 5 min, gradient at 2.1%/min for 45 min, 100% solvent B for 5 min at a flow rate of 2.5 μl/min. The MS conditions were as follows: ion spray voltage 3.0 kV, electron multiplier voltage 2400 V, curtain gas nitrogen 10 for MS and MS/MS analysis; collision gas, nitrogen 10, and collision energy, 20–25 eV for MS/MS analysis. To identify the proteins, peptide mapping of the 150 kDa band was performed by LC-MS using the PROWL (ProFound) search engine (prowl.rockefeller.edu/cgi-bin/ProFound) and the public domain database (NCBI) available on the internet. The major ion peaks of the total ion chromatogram were further analysed to obtain the amino acid sequences of the trypsinized peptides by LC-MS/MS using the Mascot search engine (www.matrixscience.com) under the same conditions (QSTAR with Magic micro LC) and the same database.

The nitrated tyrosine residues in the peptides were identified by single-ion monitoring (SIM) using $[M+2H]^{2+}$ and $[M+45(NO_2)+2H]^{2+}$ ions. The nitrated tyrosine peptides appeared on the chromatogram at 30–150 s after the unmodified tyrosine peptides [16].

Statistical analysis. All results are expressed as means ± SEM. Differences between groups were examined for significance using Student's *t* test and a *P* value of less than 0.05 was taken to indicate the presence of a significant difference.

Results

Peroxynitrite impairs insulin-stimulated glucose uptake

To investigate the effects of peroxynitrite on insulin-stimulated glucose uptake, we incubated 3T3-L1 adipocytes with various concentrations of SIN-1 for 12 h (Fig. 1) and then measured glucose uptake using 2-deoxyglucose as a tracer. SIN-1 simultaneously generates superoxide and NO, thus peroxynitrite is produced by

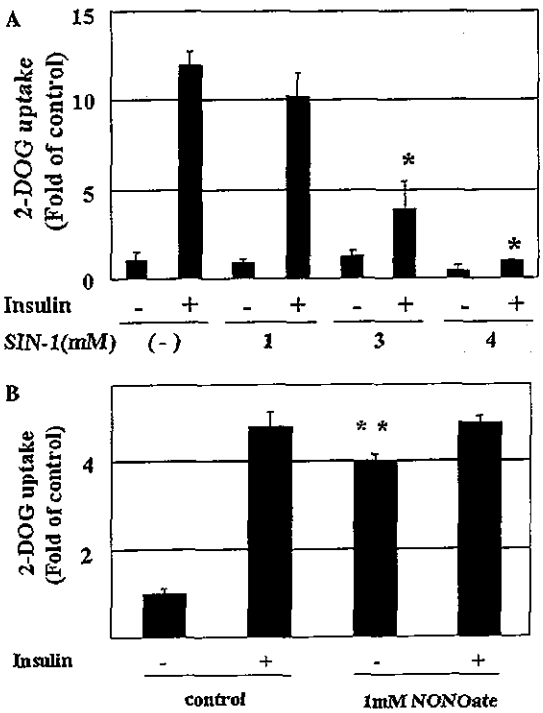

Fig. 1. Effects of peroxynitrite on insulin-stimulated 2-deoxyglucose uptake. (A) 3T3-L1 adipocytes were incubated with or without the indicated concentrations of SIN-1 for 12 h. (B) 3T3-L1 adipocytes were incubated with or without 1 mM spermine NONOate for 12 h. Then cells were stimulated with 100 nM insulin for 1 h after which 2-deoxyglucose uptake was measured as described in Materials and methods. The results were corrected by the protein concentration. 2-Deoxyglucose uptake was expressed relative to that by cells incubated in the absence of insulin and SIN-1. All experiments were performed in duplicate on five separate occasions. Data are means ± SEM. Statistical significance was determined by Student's *t* test. $^*p < 0.05$ compared with insulin-stimulated control cells. $^{**}p < 0.05$ compared with insulin-unstimulated control cells.

rapid chemical reaction in treated cells. In unstimulated adipocytes, treatment with SIN-1 did not cause a significant change of glucose uptake. On the other hand, treatment with SIN-1 induced significant dose-dependent inhibition of insulin-stimulated glucose uptake (control, 11.93 ± 0.78; SIN-1 at 1 mM, 10.20 ± 1.27; SIN-1 at 3 mM, 3.84 ± 1.58; and SIN-1 at 4 mM, 0.92 ± 0.06. Note: values are expressed relative to the 2-deoxyglucose uptake by cells without insulin or SIN-1 treatment, Fig. 1A).

Next, to confirm that the effect of SIN-1 on insulin signalling is caused by peroxynitrite rather than by the intermediate product, NO, we treated differentiated 3T3-L1 adipocytes with 1 mM spermine NONOate which is a constitutive NO producer, for 12 h. NO stimulated glucose uptake without insulin (Fig. 1B). Glucose uptake stimulated by insulin was not different in adipocytes treated with and without NONOate (Fig. 1B) as described previously [17]. These data indicate that peroxynitrite not NO impairs insulin-stimulated glucose uptake.

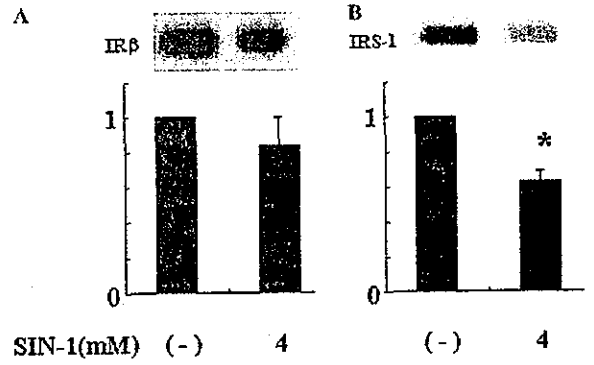

Fig. 2. Effects of peroxynitrite on insulin receptor and IRS-1 protein levels. 3T3-L1 adipocytes were serum-starved and incubated with or without 4 mM SIN-1 for 12 h. Cell extracts were immunoblotted with anti-insulin receptor antibody (A) or anti-IRS-1 antibody (B). Results are from three independent experiments. The intensity of each band was quantitated relative to the band for cells incubated in the absence of SIN-1. Data are means ± SEM. Statistical significance was determined by Student's t test. $^*p < 0.05$ compared with insulin-stimulated control cells.

Peroxynitrite impairs IRS-1-associated PI3-kinase activity

The next series of experiments were designed to determine the target molecule for peroxynitrite-induced changes of glucose uptake. For this purpose, 3T3-L1 adipocytes were cultured with 4 mM SIN-1 and SIN-1-induced changes of the insulin-signalling pathway were investigated. SIN-1 decreased the IRS-1 protein level by 38%, but not the insulin receptor level (Fig. 2). Thus, the decrease of insulin-stimulated glucose uptake by SIN-1 treatment seemed to be at least partly caused by the decrease of IRS-1 protein. To investigate other modifications of the insulin signal transduction pathway by peroxynitrite, we measured insulin-stimulated tyrosine phosphorylation using a similar amount of immunoprecipitated IRβ or IRS-1 protein to SIN-1-untreated cells. Peroxynitrite did not cause a significant change of insulin-stimulated tyrosine phosphorylation of the insulin receptor (Fig. 3A). On the other hand, SIN-1 suppressed insulin-induced stimulation of tyrosine phosphorylation of IRS-1 by 43% (control, 5.57 ± 1.76; SIN-1, 3.13 ± 0.97, Fig. 3B). SIN-1 also decreased the insulin-stimulated activation of IRS-1-associated p85, a

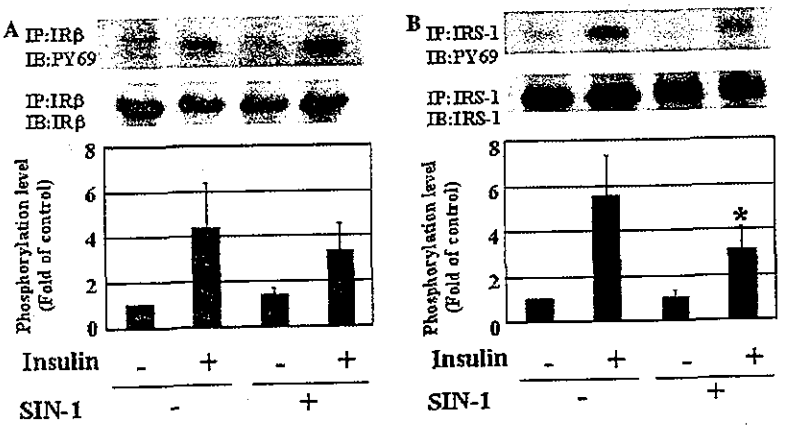

Fig. 3. Effects of peroxynitrite on phosphorylation of the insulin receptor and IRS-1. 3T3-L1 adipocytes were serum-starved and incubated with or without 4 mM SIN-1 for 12 h. Cells were stimulated with 100 nM insulin for 5 min. The cell lysates were immunoprecipitated with anti-insulin receptor β antibody (A) or anti-IRS-1 antibody (B), and then immunoblotted with anti-phosphotyrosine antibody (PY 69) (A,B). Results are from three independent experiments. The intensity of each band was quantitated relative to the band for cells incubated in the absence of insulin and SIN-1. Data are means ± SEM. Statistical significance was determined by Student's t test. $^*p < 0.05$, compared with insulin-stimulated control cells. All blots were stripped and then reprobed with anti-insulin receptor β antibody (A) or anti-IRS-1 antibody (B) to confirm that similar amounts of proteins were applied to each lane.

regulatory subunit of PI-3 kinase reducing it by 76% (Control, 9.29 ± 2.04; SIN-1 2.60 ± 0.61, Fig. 4A). In agreement with the Western blotting data, insulin-stimulated IRS-1-associated PI3-kinase activity was also markedly decreased in SIN-1-treated 3T3-L1 adipocytes (Control 12.52 ± 4.15; SIN-1 3.18 ± 0.78, Fig. 4B). Reflecting the decrease of IRS-1-associated PI3-kinase activity, SIN-1 markedly decreased insulin-stimulated serine and threonine phosphorylation of Akt (Figs. 5A and B). On the other hand, SIN-1 only induced a modest decrease of the insulin-stimulated tyrosine/threonine-phosphorylation of Erk. The associated increase of basal Erk phosphorylation might be due to the effect of increased oxidative stress on the cells (Fig. 5C). While peroxynitrite decreased the level of IRS-1 protein, independent of this fall in the protein level, peroxynitrite also impaired the insulin-stimulated phosphorylation of IRS-1, i.e., peroxynitrite reduced glucose uptake by insulin-stimulated 3T3-L1 adipocytes through impairment of downstream signals.

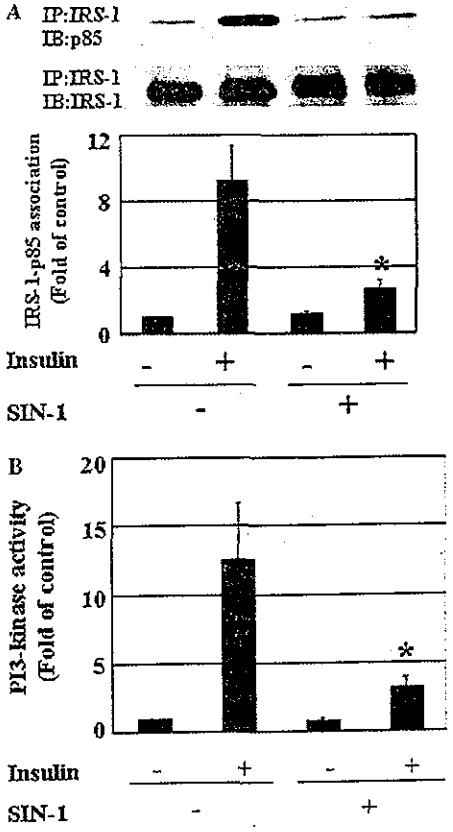

Fig. 4. Peroxynitrite impairs IRS-1-associated PI3-kinase activity. (A) 3T3-L1 adipocytes were incubated in serum-free medium with or without 4 mM SIN-1 for 12 h. Cells were stimulated with 100 nM insulin for 20 min. Cell lysates were immunoprecipitated with anti-IRS-1 antibody and then immunoblotted with anti-p85 antibody. Results are from at least three independent experiments. The intensity of each band was quantitated relative to the band for cells incubated in the absence of insulin and SIN-1. Data are means ± SEM. All blots were stripped and reprobed with anti-IRS-1 antibody to confirm that similar amounts of proteins were applied to each lane. (B) 3T3-L1 adipocytes were incubated in serum-free medium with or without 4 mM SIN-1 for 12 h and then stimulated with 100 nM insulin for 20 min. The cell lysates were immunoprecipitated with anti-IRS-1 antibody. Experiments were performed in triplicate on three separate occasions. The immunoprecipitates were subjected to PI3-kinase assay using phosphatidylinositol as a substrate. The intensity of each band was quantitated relative to that of cells incubated in the absence of insulin and SIN-1. Data are means ± SEM. Statistical significance was determined by Student's t test. $^{*}p < 0.05$ compared with insulin-stimulated control cells.

Peroxynitrite induces tyrosine nitration of IRS-1 but not Ser^{307}-phosphorylation of IRS-1

To further investigate the mechanism(s) of the effects of peroxynitrite on insulin signalling, we assessed whether treatment with SIN-1 could induce phosphorylation of the Ser^{307} residues of IRS-1. Ser^{307} phosphorylation of IRS-1 was detected in TNF-α-treated cells but not in SIN-1-treated cells (Fig. 6A). These results demonstrated that phosphorylation of the Ser^{307} residues of IRS-1 is not involved in the impairment of insulin signalling by peroxynitrite. Peroxynitrite is known to induce the nitration of Tyr of several molecules. Thus, we investigated tyrosine nitration of IRS-1 in SIN-1-treated 3T3-L1 adipocytes. In 3T3-L1 adipocytes, only a modest tyrosine nitration of IRS-1 could be detected (data not shown). Therefore, we investigated tyrosine nitration of IRS-1 in SIN-1-treated HIRc. Different from 3T3-L1 adipocytes, SIN-1-treated HIRc does not show the decrease in the level of IRS-1 protein (Fig. 6B). In these cells, Ser^{307} phosphorylation of IRS-1 was also not detected, but tyrosine nitration of IRS-1 was detected in both 4 and 8 mM SIN-1 (Fig. 6C). In TNF-α-treated cells, where we found the induction of iNOS expression (data not shown), both Ser^{307} phosphorylation and tyrosine nitration of IRS-1 were detected (Fig. 6C).

Detection of nitrated tyrosine residue of peroxynitrite-treated IRS-1

To investigate the relation between peroxynitrite-induced tyrosine nitration of IRS-1 and impairment of insulin signal pathway, recombinant rat IRS-1 was incubated with 50 μM peroxynitrite for 1 h. As shown in Fig. 7A, tyrosine nitration of rat IRS-1 was clearly detected by Western blotting (an approximately 150 kDa band). Next, we investigated the nitrated tyrosine residues of IRS-1 after peroxynitrite treatment by MS. After in-gel digestion of the band stained with CBB, peptide mapping was carried out. A total of 25 trypsinized peptides of IRS-1 were identified by LC-MS and the PROWL search engine. The amino acids covered 31.5% of the whole sequence of IRS-1 (389/1235). The amino acid sequences of six peptides were also

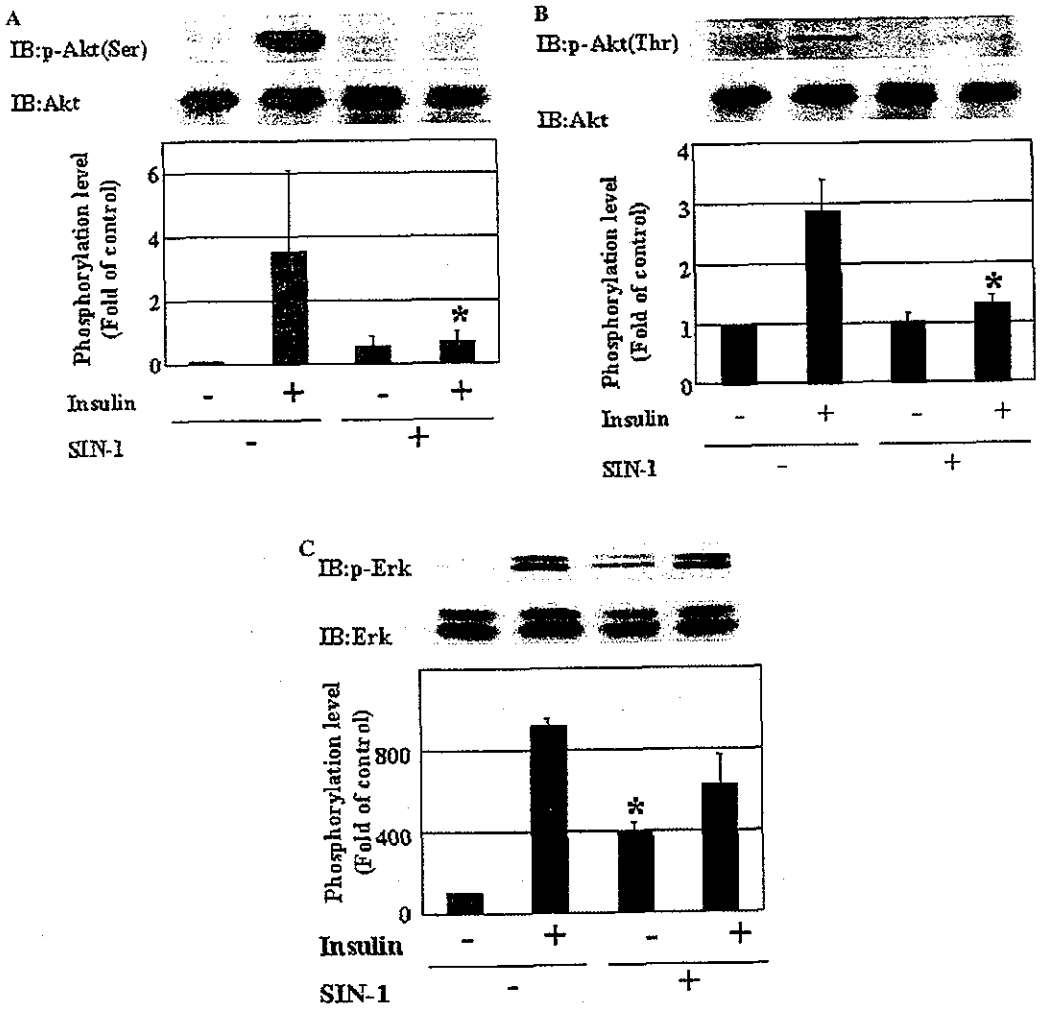

Fig. 5. Effects of peroxynitrite on phosphorylation of Akt and Erk. Differentiated 3T3-L1 adipocytes were incubated in serum-free medium with or without 4 mM SIN-1 for 12 h. Cells were stimulated with 100 nM insulin for 20 min and then immunoblotted with anti-serine (473) phosphospecific Akt antibody (A), anti-threonine (308) phosphospecific Akt antibody (B), and anti-phosphospecific Erk antibody (C). Results are from three independent experiments. The intensity of each band was quantitated relative to the band for cells incubated in the absence of insulin and SIN-1. Data are means ± SEM. Statistical significance was determined by Student's t test. $^*p < 0.05$ compared with insulin-stimulated control cells. The bands were stripped and reprobed with anti-Akt antibody (A,B) or anti-Erk antibody (C).

confirmed by LC-MS/MS and the MASCOT search engine (6.2% of IRS-1) (Table 1). We found four unique peptides, the tyrosine of which residues was nitrated by peroxynitrite. These were detected by SIM of peptide mapping at the ion of $[M+2H]^{2+}$ and $[M+45+2H]^{2+}$ because increase of 45 Da corresponded to the NO_2 group. Modified peptides also appeared at 30–150 s behind the unmodified protein (Fig. 7B). The four peptides at residues 489–515 (Tyr^{489}), 932–948 (Tyr^{939}), 997–1014 (Tyr^{999} or Tyr^{1010}), and 1169–1179 (Tyr^{1172}) were identified as peptides containing nitrated tyrosine (Table 1). The ratio of modified to unmodified peptides was 4.1% at Tyr^{489}, 26.9% at Tyr^{939}, 8.0% at Tyr^{999} or Tyr^{1010}, and 35.3% at Tyr^{1172} (Table 1). The residues at Tyr^{939} and Tyr^{1172} were identified as the phosphorylation site of IRS-1 according to the SWISS-PROT database and seemed to be more easily nitrated than Tyr^{489} and Tyr^{999} or Tyr^{1010}. These results demonstrate that at least two of the phosphorylation sites of the tyrosine residues of IRS-1 could be nitrated by exposure to peroxynitrite.

Discussion

Insulin receptor substrate (IRS) proteins are essential signalling molecules that mediate the metabolic actions of insulin and, IRS-1 and -2 are recognized as especially important molecules in glucose metabolism [18]. The activated insulin receptor-related tyrosine kinase phosphorylates multiple tyrosine residues of

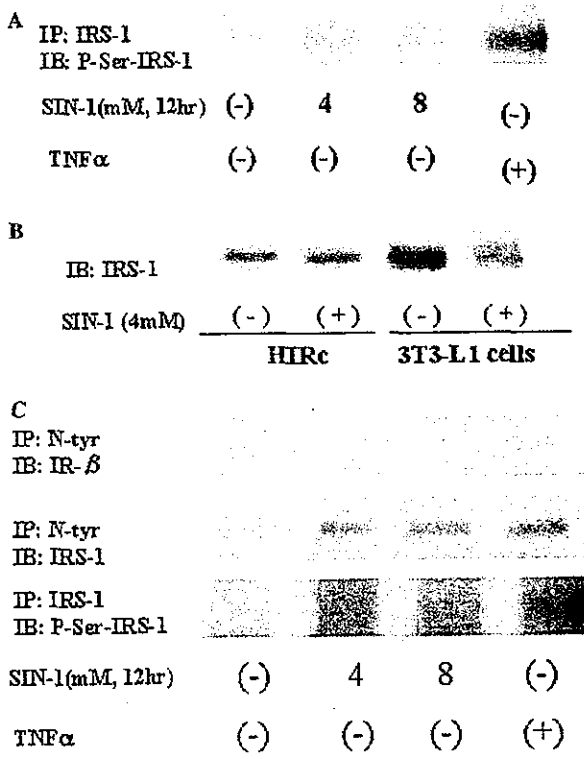

Fig. 6. Peroxynitrite induces tyrosine nitration of IRS-1, but not serine phosphorylation of IRS-1. (A) 3T3-L1 adipocytes were incubated with 0, 4 or 8 mM SIN-1 for 12 h, or with 50 ng/ml TNF-α 48 h. The cell lysates were immunoprecipitated with anti-nitrotyrosine or anti-IRS-1 antibody and then immunoblotted with anti-phosphoserine (307)-IRS-1 antibody, anti-insulin receptor β antibody or anti-IRS-1 antibody. (B) 3T3-L1 adipocytes and HIRc were incubated with 0 or 4 mM SIN-1 for 12 h. The cell lysates were used for immunoblotting with anti-IRS-1 antibody. (C) HIRc were incubated with 0, 4 or 8 mM SIN-1 for 12 h, or with 50 ng/ml TNF-α 48 h. The cell lysates were immunoprecipitated with anti-nitrotyrosine or anti-IRS-1 antibody and then immunoblotted with anti-phosphoserine (307)-IRS-1 antibody, anti-insulin receptor β antibody or anti-IRS-1 antibody. This figure shows representative data from three independent experiments.

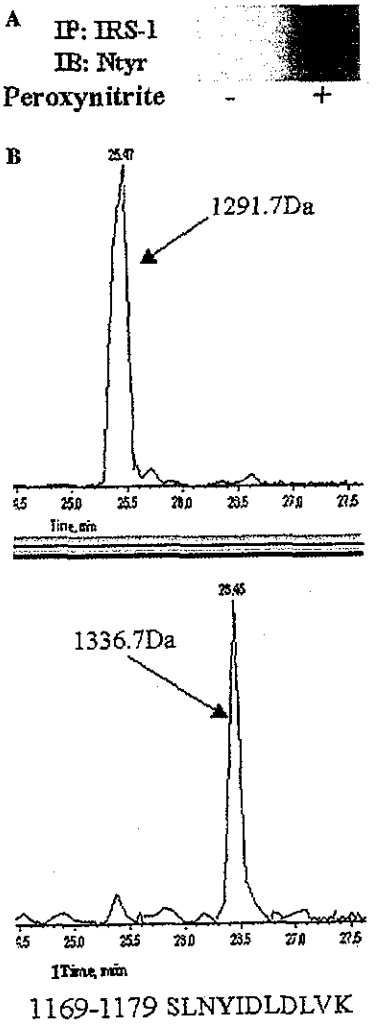

Fig. 7. Identification of nitrated tyrosine residues of rat IRS-1 after exposure to peroxynitrite. (A) One milligram of rat recombinant IRS-1 was incubated with or without 50 μM peroxynitrite for 1 h at 4 °C. Then the sample was immunoprecipitated with anti-IRS-1 antibody and immunoblotted with anti-nitrotyrosine antibody. (B) Representative SIM profiles of peroxynitrite-modified and unmodified peptides. The monitoring ions of both peptides at residues 1169–1179 ($SLNY^{1172}IDLDLVK$) are *m/z* 646.8 as the $[M+2H]^{2+}$ ion (*top*) and *m/z* 669.3 as the $[M+45+2H]^{2+}$ ion (bottom). The molecular weights of the peptides were 1291.7 and 1336.7 Da.

IRS proteins that act as docking sites for downstream mediators. Among these mediators, PI3-kinase plays an important role in the metabolic actions of insulin and it binds to IRS-1 at its phosphorylated $Tyr^{608}$and Tyr^{939} [19]. IRS-1 is also a substrate for various serine kinases, including c-Jun NH_2-terminal kinase [20], Akt [21], inhibitor κB kinase [8], and protein kinase C [22]. Activation of these kinases by TNF-α or other factors results in impairment of the insulin-signalling pathway and leads to the insulin resistance observed in obesity and type 2 diabetes [23]. In the present study, we investigated the effect of peroxynitrite, which is generated by induction of iNOS, on insulin-stimulated glucose uptake. The importance of iNOS for insulin resistance in vivo is supported by previous studies using iNOS gene-disrupted mice. In these mice, a decrease of IRS-1 phosphorylation by a high-fat diet was prevented [10]. Our data showed that peroxynitrite, which is an end-product of iNOS, inhibited insulin-induced glucose uptake, coincident with the tyrosine nitration of IRS-I. Thus, our findings suggested that tyrosine nitration of IRS-1 might also contribute to insulin resistance as does serine phosphorylation of this protein.

We found a decrease of the IRS-1 protein level and IRS-1-mediated signal transduction after treatment with SIN-1. Previous studies have demonstrated that tyrosine-nitrated proteins are more easily degraded [6], thus,

Table 1
Identification of trypsinized peptides of IRS-1 and confirmation of the nitrated tyrosine residues of IRS-1 following treatment with peroxynitrite

Residue	No.	Sequence	Identification of IRS-1		Nitration of Tyr	
			PROWL MS	MASCOT MS/MS	$[M+45+2H]^{2+}$ SIM	NO_2 (%) modification
29–33	5	FFVLR	○			
44–51	8	LEYYENEK	○			
82–89	8	HLVALYTR	○	○		
157–166	10	EVWQVILKPK	○	○		
167–172	6	GLGQTK	○			
173–179	7	NLIGIYR	○			
192–207	16	LNSEAAAVVLQLMNIR	○	○		
223–253	31	SAVTGPGEFWMQVDDSVVAQNMHETILEAMR	○			
282–296	15	HHLNNPPPSQVGLTR	○			
300–315	16	TESITATSPASMVGGK	○			
316–320	5	PGSFR	○			
489–515	27	YIPGATMGTSPALTGDEAAGAADLDNR	○		○	4.1
520–533	14	THSAGTSPTISHQK	○			
534–563	30	TPSQSSVVSIEEYTEMMPAAYPPGGGSGGR	○			
635–647	13	SVSAPQQIINPIR	○	○		
820–838	19	PESSVTHPHHHALQPHLPR	○			
856–862	7	LSLGDPK	○			
871–890	20	EQQQQQQQQQSSLHPPEPK	○			
932–948	17	EETGSEEYMNMDLGPGR	○	○	○	26.9
950–962	13	ATWQESGGVELGR	○	○		
976–996	21	PTRSVPNSRGDYMTMQIGCPR	○			
997–1014	18	QSYVDTSPVAPVSYADMR	○		○	8.0
1022–1026	5	VSLPR	○			
1027–1073	47	TTGAAPPPSSTASASASVTPQGAAEQAAHSSLL GGPQGPGGMSAFTR	○			
1169–1179	11	SLNYIDLDLVK	○		○	35.3
		Total residues (1235)	389	77		
		Coverage	31.5%	6.2%		

A mixture of trypsinized peptides was examined by peptide mapping using LC-MS and the PROWL search engine. The amino acid sequences of some peptides were confirmed using LC-MS/MS and the MASCOT search engine. The nitrated tyrosine residues were confirmed by SIM at the $[M+2H]^{2+}$ and $[M+45+2H]^{2+}$ ions. NO_2 (%) represents the ratio of the ion intensities of the modified and the unmodified tyrosine. Tyrosine residues are shown in bold type.

we speculated that tyrosine-nitrated IRS-1 may also be readily degraded. If so, the reason that we only observed a modest increase of tyrosine nitration of IRS-1 in 3T3-L1 adipocytes treated with SIN-1 (data not shown) might be due to the degradation of IRS-1. In fact, we found a definite increase of tyrosine nitration in HIRc without showing the decrease of the protein level of IRS-1. Thus, tyrosine nitration of IRS-1 may occur by direct modification due to peroxynitrite, and such modification may impair the stability of IRS-1 in a cell-dependent manner.

We used MS to identify the nitrated tyrosine residues in rat IRS-1. The rat IRS-1 protein has 34 tyrosine residues, more than 10 of which can be phosphorylated by insulin receptor tyrosine kinase. In this study, MS covered about 30% of the peptide sequence and showed that at least Tyr^{489}, Tyr^{939}, either Tyr^{999} or Tyr^{1010}, and Tyr^{1172} residues could be nitrated by peroxynitrite. Among the tyrosine residues of IRS-1, four are found in the src homology 2 (SH2)-binding domain. Among these, Tyr^{608} and Tyr^{939} are especially considered to be important tyrosine residues for docking to the p85 subunit of PI3 kinase [6]. Although we could not investigate whether Tyr^{608} was nitrated because of difficulty in isolating a digested peptide including Tyr^{608}, nitration of Tyr^{939} may also inhibit the phosphorylation of IRS-1 at this site and might be involved in the impairment of IRS-1-associated PI3-kinase activity. We showed that treatment with SIN-1 led to the suppression of IRS-1 phosphorylation and more marked suppression of IRS-1-associated p85 activity. These findings suggest that nitration of the tyrosine residues of IRS-1 inhibits tyrosine phosphorylation by the insulin receptor, and thus inhibits its association with p85.

SIN-1 caused more dramatic suppression of IRS-1-associated p85 activity than IRS-1 phosphorylation possibly due to the impairment of PI-3 kinase. Hellberg et al. [24] reported that spermine NONOate, a NO donor, induced tyrosine nitration of the p85 subunit of PI3-kinase in a macrophage cell line. We also detected a modest increase of tyrosine nitration of the p85 subunit together with a modest decrease of the interaction between p85 and

p110. (T.N. and H.W., unpublished observation). Taken together, it is conceivable that various molecules, including p85, are probably involved in the NO-induced reduction of insulin-stimulated glucose uptake. Among these, IRS-1 is certainly the most upstream molecule and one of the most important targets of peroxynitrite in the insulin-signalling cascade (Fig. 4B).

Peroxynitrite is produced by the reaction of NO with superoxide. High blood levels of free fatty acids and glucose, which are often found in diabetes and obesity, can induce the production of superoxide through various mechanisms including increased uptake of substrates by the mitochondria [25]. Thus, once iNOS is induced in insulin-sensitive tissues, peroxynitrite may be easily generated from NO in obese and diabetic individuals. Clinical studies have demonstrated the presence of nitrotyrosine in the blood of diabetic patients, and its level increases in hyperglycaemia [26].

In conclusion, the present study identified a possible mechanism of insulin resistance, which is the main etiopathological factor of type 2 diabetes and multiple risk factor syndrome. Inhibition of the tyrosine nitration of IRS-1 could be a potentially useful therapeutic target for the treatment of diabetes and related diseases.

Acknowledgments

We thank Dr. J.M. Olefsky for providing HIRc and Drs. K. Egawa, T. Fujita, K. Morino (Shiga University of Medical Science, Otsu, Japan), and F. Yamakura (Juntendo University, Chiba) for the helpful discussion. We also thank Naoko Daimaru for the excellent technical assistance. This work was supported by grants from the Juvenile Diabetes Research Foundation International (to H.W.), the Ministry of Education, Sports and Culture of Japan (to H.U.), and the Takeda Science Foundation (to R.K.).

References

[1] H.O. Steinberg, G. Brechtel, A. Johnson, N. Fineberg, A.D. Baron, J. Clin. Invest. 94 (1994) 1172–1179.
[2] K.Q. Do, G. Grima, B. Benz, T.E. Salt, Ann. N. Y. Acad. Sci. 962 (2002) 81–92.
[3] C. Nathan, J. Clin. Invest. 100 (1997) 2417–2423.
[4] D.O. Stichtenoth, J.C. Frolich, Br. J. Rheumatol. 37 (1998) 246–257.
[5] R.E. Huie, S. Padmaja, Free Radic. Res. Commun. 18 (1993) 195–199.
[6] A.J. Gow, D. Duran, S. Malcolm, H. Ischiropoulos, FEBS Lett. 385 (1996) 63–66.
[7] X. Li, P. De Sarno, L. Song, J.S. Beckman, R.S. Jope, Biochem. J. 331 (Pt. 2) (1998) 599–606.
[8] Z. Gao, D. Hwang, F. Bataille, M. Lefevre, D. York, M.J. Quon, J. Ye, J. Biol. Chem. 277 (2002) 48115–48121.
[9] S. Kapur, B. Marcotte, A. Marette, Am. J. Physiol. 276 (1999) E635–E641.
[10] M. Perreault, A. Marette, Nat. Med. 7 (2001) 1138–1143.
[11] P.M. Sharma, K. Egawa, T.A. Gustafson, J.L. Martin, J.M. Olefsky, Mol. Cell. Biol. 17 (1997) 7386–7397.
[12] A. Klip, G. Li, W.J. Logan, Am. J. Physiol. 247 (1984) E291–E296.
[13] T. Ogihara, H. Watada, R. Kanno, F. Ikeda, T. Nomiyama, Y. Tanaka, A. Nakao, M.S. German, I. Kojima, R. Kawamori, J. Biol. Chem. 278 (2003) 21693–21700.
[14] R. Mineki, H. Taka, T. Fujimura, M. Kikkawa, N. Shindo, K. Murayama, Proteomics 2 (2002) 1672–1681.
[15] U.K. Laemmli, Nature 227 (1970) 680–685.
[16] F. Yamakura, H. Taka, T. Fujimura, K. Murayama, J. Biol. Chem. 273 (1998) 14085–14089.
[17] M.E. Young, G.K. Radda, B. Leighton, Biochem. J. 322 (Pt. 1) (1997) 223–228.
[18] A.R. Saltiel, C.R. Kahn, Nature 414 (2001) 799–806.
[19] X.J. Sun, D.L. Crimmins, M.G. Myers Jr., M. Miralpeix, M.F. White, Mol. Cell. Biol. 13 (1993) 7418–7428.
[20] V. Aguirre, T. Uchida, L. Yenush, R. Davis, M.F. White, J. Biol. Chem. 275 (2000) 9047–9054.
[21] J. Li, K. DeFea, R.A. Roth, J. Biol. Chem. 274 (1999) 9351–9356.
[22] L.V. Ravichandran, D.L. Esposito, J. Chen, M.J. Quon, J. Biol. Chem. 276 (2001) 3543–3549.
[23] S. Mora, J.E. Pessin, Diabetes Metab. Res. Rev. 18 (2002) 345–356.
[24] C.B. Hellberg, S.E. Boggs, E.G. Lapetina, Biochem. Biophys. Res. Commun. 252 (1998) 313–317.
[25] T. Nishikawa, D. Edelstein, X.L. Du, S. Yamagishi, T. Matsumura, Y. Kaneda, M.A. Yorek, D. Beebe, P.J. Oates, H.P. Hammes, I. Giardino, M. Brownlee, Nature 404 (2000) 787–790.
[26] A. Ceriello, F. Mercuri, L. Quagliaro, R. Assaloni, E. Motz, L. Tonutti, C. Taboga, Diabetologia 44 (2001) 834–838.

Available online at www.sciencedirect.com
SCIENCE DIRECT®
Biochemical and Biophysical Research Communications 317 (2004) 162–168
BBRC
www.elsevier.com/locate/ybbrc

Hypoxia followed by reoxygenation induces secretion of cyclophilin A from cultured rat cardiac myocytes☆

Yoshinori Seko,[a,*] Tsutomu Fujimura,[b] Hikari Taka,[b] Reiko Mineki,[b] Kimie Murayama,[b] and Ryozo Nagai[a]

[a] *Department of Cardiovascular Medicine, Graduate School of Medicine, University of Tokyo, Bunkyo-ku, Tokyo, Japan*
[b] *Division of Proteomics and Biomolecular Science, BioMedical Research Center, Graduate School of Medicine, Juntendo University, Bunkyo-ku, Tokyo, Japan*

Received 18 February 2004

Abstract

We previously reported that hypoxia followed by reoxygenation (hypoxia/reoxygenation) rapidly activated intracellular signaling such as mitogen-activated protein kinases (MAPKs) including extracellular signal-regulated protein kinase (ERK) 1/2, p38MAPK, and stress-activated protein kinases (SAPKs). To investigate the humoral factors which mediate cardiac response to hypoxia/reoxygenation, we analyzed the conditioned media from cardiac myocytes subjected to hypoxia/reoxygenation by two-dimensional electrophoresis and mass spectrometry. We identified cyclophilin A (CyPA) as one of the proteins secreted from cardiac myocytes in response to hypoxia/reoxygenation. Hypoxia/reoxygenation induced the expression of CyPA and its cell surface receptor CD147 on cardiac myocytes in vitro. This was also confirmed by ischemia/reperfusion in vivo. Recombinant human (rh) CyPA activated ERK1/2, p38MAPK, SAPKs, and Akt in cultured cardiac myocytes. Furthermore, CyPA significantly increased Bcl-2 in cardiac myocytes. These data strongly suggested that CyPA is released from cardiac myocytes in response to hypoxia/reoxygenation and may protect cardiac myocytes from oxidative stress-induced apoptosis.

Keywords: Apoptosis; Autocrine; Cardiac myocyte; CD147; Cyclophilin; Hypoxia; Ischemia; Reoxygenation; Reperfusion; Signal transduction

We previously reported that both hypoxia and hypoxia followed by reoxygenation (hypoxia/reoxygenation) rapidly and sequentially activated mitogen-activated protein kinase kinase kinase (MAPKKK) activity of Raf-1, MAP kinase kinase (MAPKK), MAPKs ($p44^{mapk}$ and $p42^{mapk}$) (also called extracellular signal-regulated protein kinase [ERK]1 and ERK2, respectively), and S6 kinase ($p90^{rsk}$) as well as Src family tyrosine kinases (c-Src and c-Fyn) and $p21^{ras}$, which are upstream mediators of MAPK pathway [1,2]. We also reported that both hypoxia and hypoxia/reoxygenation rapidly activated stress-activated MAPK signaling cascades involving $p65^{PAK}$, p38MAPK, and stress-activated protein kinases (SAPKs) in cultured rat cardiac myocytes [3]. Activation of these signaling cascades results in the expression of various genes coding for growth factors, cytokines, cell-adhesion molecules, and so on, which may play a role in the adaptation to these stresses or lead to further cell damage known as reperfusion injury. In this study, to investigate the humoral factors which mediate cardiac response to hypoxia/reoxygenation, we analyzed the conditioned media from cardiac myocytes subjected to hypoxia/reoxygenation and found that cyclophilin A (CyPA) was secreted from cardiac myocytes and might

☆ *Abbreviations:* BPB, bromophenol blue; CBB, Coomassie brilliant blue; CyPA, cyclophilin A; 2-D, two dimensional; DMEM, Dulbecco's modified Eagle's medium; DTE, dithioerythritol; ERK, extracellular signal-regulated protein kinases; HIV, human immunodeficiency virus; IEF, isoelectric focusing; MAPK, mitogen-activated protein kinase; MAPKK, MAPK kinase; MAPKKK, MAPK kinase kinase; MS, mass spectrometry; PBS, phosphate-buffered saline; PDA, piperazine diacrylamide; SAPK, stress-activated protein kinase; SDS–PAGE, sodium dodecyl sulfate–polyacrylamide gel electrophoresis; Ser, serine; TCA, trichloroacetic acid; TRITC, tetramethyl rhodamine isothiocyanate; TSA, tyramide signal amplification; Tyr, tyrosine; Thr, threonine; VSMC, vascular smooth muscle cell.

* Corresponding author. Fax: +81-3-5689-3815.
E-mail address: sekoyosh-tky@umin.ac.jp (Y. Seko).

0006-291X/$ - see front matter © 2004 Elsevier Inc. All rights reserved.
doi:10.1016/j.bbrc.2004.03.021

play a role in protecting cardiac myocytes from oxidative stress-induced cell injury.

Materials and methods

Cell culture. Primary cultures of ventricular cardiac myocytes were prepared from neonatal rats as previously described [1]. They were cultured for two days until they were confluent and then serum-starved for 24 h before use.

Hypoxia and reoxygenation. Hypoxic condition (95% N_2, 5% CO_2, and less than 0.1% O_2) was achieved by using an anaerobic jar equipped with a new type AnaeroPack (disposable O_2 absorbing and CO_2 generating agent, Mitsubishi Gas Chemical, Japan) and an indicator to monitor oxygen depletion as described previously [1]. By placing flasks, which contain phosphate-buffered saline (PBS), in an anaerobic jar overnight, the PBS was balanced with the hypoxic atmosphere. Cultured cardiac myocytes were subjected to a hypoxic condition by immediately replacing the medium with the hypoxic PBS in an anaerobic jar. To keep hypoxic conditions, all the procedures were performed in a glove bag filled with 95% N_2 and 5% CO_2. After incubating in a hypoxic condition for 60 min, the cells were reoxygenated by immediately replacing the hypoxic PBS with normoxic PBS for the indicated time periods. We collected the supernatant PBS after 10 min of reoxygenation as reoxygenation-conditioned PBS. We also collected the supernatant PBS after 10 min of incubation with non-stimulated cardiac myocytes under normoxia as control-conditioned PBS.

Two-dimensional gel electrophoresis. We concentrated the reoxygenation-conditioned PBS and control-conditioned PBS by using centripreps (YM-10; Millipore, Bedford, MA, USA) and collected the fractions of molecular weight >10 kDa from them. Immobiline dry strips at pH 3–10 (7 cm), IPG buffer, PlusOne silver staining kit, and Coomassie brilliant blue (CBB-R350) were purchased from Amersham Biosciences (Uppsala, Sweden). For the first-dimensional isoelectric focusing (IEF), IPGphor strips (7 cm) at pH 3–10 were used. The concentrated-conditioned PBS (50 μg/125 μl) in a microtube (Treff AG, Schweiz, Switzerland) was diluted with Milli Q water (375 μl) and deproteinized with the 500 μl of 40% trichloroacetic acid (TCA) (final concentration 20%). The mixtures were allowed to stand on ice for more than 1 h and centrifuged at 13,000 rpm for 10 min. The supernatants were discarded and the precipitates were washed with cold ether three times to remove excess TCA. The final precipitates were dissolved in the IEF solution containing 9 M urea, 4% CHAPS, 65 mM dithioerythritol (DTE), 2% IPG buffer, pH 3–10, and bromophenol blue (BPB). The dried IPG strips were rehydrated overnight in the sample solution. Then, IEF was performed with the following steps; increasing voltage 30 V for 7 h, 60 V for 7 h, from 60 to 200 V for 0.5 h, from 200 to 500 V for 0.5 h, from 500 to 1000 V for 0.5 h, from 1000 to 8000 V for 0.5 h, and held at 8000 V for 1 h, i.e., a total of 11.5 kV h. Before loading on a 2-D SDS–PAGE, the IPG strips were immersed in 5 ml solution containing 50 mM Tris–HCl (pH 8.5), 6 M urea, 30% glycerol, 2% SDS, 150 mM DTE, and 0.005% BPB and were shaken slowly for 10 min at room temperature in order to reduce the inner and intra-disulfide bonds of cysteinyl residues. And then, the reduced proteins were alkylated with 5 ml of 300 mM acrylamide at room temperature for 10 min. For the 2-D sodium dodecyl sulfate–polyacrylamide gel electrophoresis (SDS–PAGE), we used a gel (110 × 110 × 1 mm; Nihon Eido, Tokyo, Japan), which was prepared for separating gel (10% acrylamide and 2.6% piperazine diacrylamide [PDA]) and for stacking gel (4% acrylamide and 2.6% PDA). The prerun was performed at 24 mA for 45 min to remove the excess reagents and adjust gel condition. The IPG strips were placed onto the surface of a stacking gel. At first, the 2-D SDS–PAGE commenced at 6 mA for 30 min in order to release proteins from the IPG strips and to stack those into the 2-D gel. Subsequently, the proteins were separated at 12 mA for 3.25 h. The proteins in the gels were stained with the silver staining kit or the CBB R-350 reagent kit and profiled with the image analyzer, Master Scan (Scanalytics, Billerica, MA, USA).

In gel digestion. The proteins on the 2-D SDS–PAGE were subjected to in gel digestion as described previously [4]. The spots were excised manually using a razor blade, placed in microtubes, washed with H_2O (10 min, 37 °C, five times), and destained in 100 μl of 50% CH_3CN and 100 mM ammonium bicarbonate (pH 8.5) for 10 min at 37 °C until colorless. The gels were dehydrated in 100 μl CH_3CN in a microtube for 10 min at 37 °C and was dried in Micro Vac MV-100 (Fomy, Tokyo, Japan) for 5 min. The dried residue was rehydrated by adding 50 μl of 0.001% trypsin in 100 mM ammonium bicarbonate (pH 8.5) and incubated overnight at 37 °C. The incubation mixture in the microtube was centrifuged, and the residue was extracted with 50% CH_3CN and 0.1% trifluoroacetic acid, and centrifuged again. The residue was further extracted with 15% isopropyl alcohol, 20% formic acid, 25% CH_3CN, 40% H_2O, and finally with 80% CH_3CN. The supernatant and all of the extracts were successively dried in a single microtube, and the residue was dissolved in 6 μl of 0.1% formic acid. Aliquots were used for protein identification by mass spectrometry.

Mass spectrometry. Peptide mapping was carried out using API QSTAR Pulsar (I) hybrid mass spectrometer system with a microliquid chromatograph (Magic 2002, Michrom BioResource, Auburn, CA, USA). The QSTAR pulsar hybrid mass spectrometer system consists of the apparatus of nanoelectrospray ionization and the quadrupole-time of flight (ESI-TOF) mass spectrometer. Mass accuracy was ±0.1 mass unit. Conditions of mass spectrometry (MS) were as follows; ion spray voltage of 2.0–2.8 kV, voltage for the electron multiplier of 2400 V, nitrogen for curtain gas of 10, nitrogen for collision gas of 10, and collision energy of 20–55 eV for MS/MS analysis. Conditions of micro-LC were as follows; Magic C18 column (0.2 mm, inner diameter × 50 mm) and elution with 0.1% formic acid (solvent A) and 0.1% formic acid in 90% CH_3CN (solvent B) using a program of 3% solvent B for 2 min, gradient at 2.1%/min for 45 min, 100% solvent B for 5 min, and flow rate of 2.5 μl/min. Proteins in-gel digested on 2-D SDS–PAGE were identified with LC-MS/MS using the PROWL (ProFound) and Mascot search engines, and NCBI database.

Ischemia and reperfusion. Rats (male, 250–280 g) were subjected to coronary artery ligation by techniques previously described [5]. Briefly, rats were anesthetized with sodium pentobarbital (40 mg/kg, intraperitoneally), intubated, and ventilated with room air (tidal volume, 20 ml/kg at rate of 60/min) with a respirator (SN-480-7, Shinano Manufacturing, Tokyo, Japan). After lateral thoracotomy and pericardiectomy, a 6–0 silk stitch was placed near the intramyocardial location of the left coronary artery beneath the left atrial appendage. We performed coronary artery occlusion by pressing a short length of tube over the ends of the suture and clamping it firmly against the heart. We achieved reperfusion by removing the clamp. The standard limb lead II electrocardiogram was monitored continuously. We confirmed the ischemia and reperfusion of the regional myocardium by following the changes of the ST segment level on the electrocardiogram and observing the change in the color of the myocardium.

Immunohistochemistry. We used tyramide signal amplification (TSA) technology for fluorescence (TSA-Direct [Green], NEN Life Science Products, according to the manufacturer's instructions). Rats were killed at each time point after myocardial ischemia/reperfusion. Cryostat sections (6-μm thick) of heart ventricles were prepared, air-dried, and fixed in acetone for 5 min. After washing in PBS, the sections were incubated with rabbit polyclonal anti-CyPA antibody (Upstate Biotechnology, NY, USA) or goat polyclonal anti-CD147 antibody (G-19; Santa Cruz Biotechnology, CA, USA) for 1 h at 37 °C. After washing in PBS, the sections were incubated with biotinylated anti-rabbit or goat IgG antibody (Vector Laboratories, CA) for 1 h at 37 °C. After washing in TNT buffer (0.1 mol/L Tris–HCl, pH 7.5,

0.15 mol/L NaCl, and 0.05% Tween 20), the sections were blocked with TNB buffer containing a blocking reagent for 30 min and then incubated with streptavidin–horseradish peroxidase for 30 min. After washing in TNT buffer, the sections were incubated with fluorescein–tyramide for appropriate time (3–10 min), washed in TNT buffer, and then examined, and photographed under a fluorescence microscope.

Immunocytochemistry. For immunocytochemical analysis, to distinguish cardiac myocytes from non-muscle cells (mainly consisted of fibroblasts), we performed double-staining for cardiac myosin and CyPA or CD147 using a mouse anti-cardiac myosin monoclonal antibody (mAb) (CMA19) [6] and tetramethyl rhodamine isothiocyanate (TRITC)-conjugated anti-mouse IgG antibody as described previously [7]. The procedures for staining of CyPA and CD147 were the same as for the tissue samples.

Western blot analyses for phosphorylation of ERK1/2, p38MAPK, SAPKs, and Akt. Cardiac myocytes were treated with 10 nM of recombinant human (rh) CyPA (Sigma Chemical, MO, USA) for the indicated time periods, then the culture media were aspirated immediately and cardiac myocytes were frozen in liquid nitrogen. The cells were lysed on ice with buffer A and the cell lysates were centrifuged, as described previously [3]. The supernatants were suspended in Laemmli's sample buffer. Aliquots of the samples were subjected to Western blot analyses using a rabbit polyclonal phospho-specific anti-ERK1/2 (Thr202/Tyr204), p38MAPK (Tyr182), SAPKs (Thr183/Tyr185), or Akt (Ser473) antibody (New England Biolabs, MA, USA), respectively. Aliquots of the same samples were also subjected to Western blot analyses using a rabbit polyclonal control anti-ERK1/2, p38MAPK, SAPKs, or Akt antibody (New England Biolabs), respectively. The antibody–antigen complexes were developed with chemiluminescence using alkalinephosphatase (New England Biolabs).

Western blot analyses for Bcl- 2 and Bcl-X. Cardiac myocytes were treated with 50 nM rhCyPA for the indicated time periods. The procedures for preparing the Western blot samples were the same as described above. Aliquots of the samples were subjected to Western blot analyses using mouse anti-Bcl-2 or -Bcl-X mAb (Transduction Laboratories, Lexington, KY, USA). Aliquots of the same samples were subjected to Western blot analysis using a goat polyclonal anti-actin (I-19) antibody (Santa Cruz Biotechnology). The antibody–antigen complexes were developed with chemiluminescence using alkalinephosphatase.

Results

Cultured cardiac myocytes secrete CyPA in response to hypoxia/reoxygenation

Fig. 1 shows the results of 2-D gel electrophoresis of control conditioned PBS (panel A) and reoxygenation-conditioned PBS (panel B) stained with silver. A protein spot (M_r 18.2 kDa and pI 8.4) indicated by an arrow (panel B) was not present in control-conditioned PBS (panel A) and seemed to appear in response to hypoxia/reoxygenation. LC-MS/MS analysis of the protein spot identified CyPA.

Hypoxia/reoxygenation induces expression of CyPA and CD147 on cultured cardiac myocytes in vitro

Next, we examined whether cardiac myocytes express CyPA and its cell surface receptor CD147 under normal condition and in response to hypoxia/reoxygenation. Fig. 2 shows double-stained cultured cardiac myocytes under normal condition or subjected to hypoxia/reoxygenation. Panels A, B, and E show the staining pattern specific for CyPA. Panel F shows the staining pattern specific for CD147. Panels C, D, G, and H which correspond to panels A, B, E, and F, respectively, show the staining pattern specific for cardiac myosin heavy chain and indicate that most of the cells were cardiac myocytes. There was only weak expression of CyPA on cardiac myocytes under normal condition (panel A). No significant change in the expression of CyPA was seen on cardiac myocytes subjected to hypoxia for 60 min (panel B). Most of the cardiac myocytes subjected to hypoxia for 60 min followed by reoxygenation for 10 min moderately to strongly expressed CyPA on their

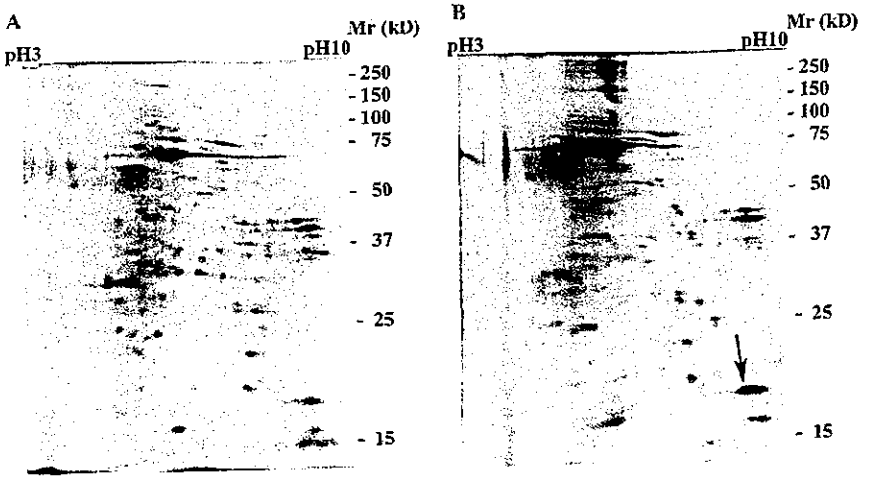

Fig. 1. 2-D gel electrophoresis of control-conditioned PBS (A) and reoxygenation-conditioned PBS (B) stained with silver. An arrow indicates a protein spot (B), which is not present in control-PBS (A).

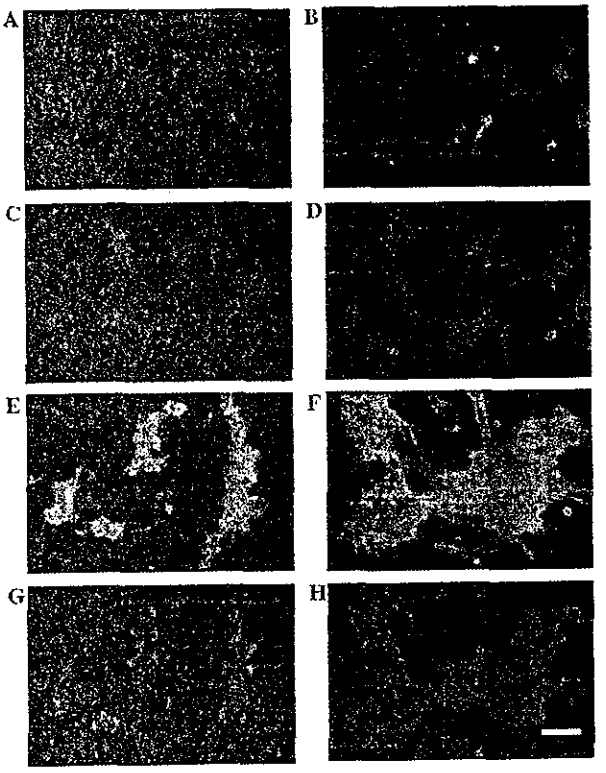

Fig. 2. Immunocytochemical study of cultured cardiac myocytes for CyPA and CD147. (A, B, E, and F) Myocytes under normal condition (A), myocytes subjected to hypoxia for 60 min (B), and myocytes subjected to hypoxia for 60 min followed by reoxygenation for 10 min (E), stained with anti-CyPA antibody, and labeled with FITC. Myocytes under normal condition (F) stained with anti-CD147 antibody and labeled with FITC. Panels C, D, G, and H which correspond to panels A, B, E, and F, respectively, show the staining pattern specific for cardiac myosin heavy chain and labeled with TRITC. Bar = 50 μm.

surfaces (panel E). Strong expression of CD147 was seen on cardiac myocytes under normal condition (panel F). The expression levels of CD147 on cardiac myocytes were not significantly changed by hypoxia or by hypoxia/reoxygenation in vitro (data not shown).

Ischemia/reperfusion induces expression of CyPA and CD147 on cardiac myocytes in vivo

To confirm the expression of CyPA and CD147 on cardiac myocytes in vivo, we examined their expression in ventricular tissues from sham-operated rats and rats subjected to myocardial ischemia/reperfusion. In sham-operated rats and rats subjected to myocardial ischemia for 30 min, there was only weak or almost no expression of CyPA on cardiac myocytes (Figs. 3A and B, respectively). In rats subjected to myocardial ischemia for 30 min followed by reperfusion for 15 min, there was a clear expression of CyPA on most of the cardiac myocytes (Fig. 3C). In sham-operated rats and rats subjected to myocardial ischemia for 30 min, there was a moderate expression of CD147 on most of the cardiac myocytes (Figs. 3D and E, respectively). Myocardial ischemia for 30 min followed by reperfusion for 30 min significantly increased the expression of CD147 on most of the cardiac myocytes (Fig. 3F).

CyPA activates ERK1/2, p38MAPK, SAPKs, and Akt in cultured cardiac myocytes

To investigate whether CyPA transduces signals through CD147 and stimulates cardiac myocytes, we examined whether rhCyPA phosphorylates MAPK family members ERK1/2, p38MAPK, and SAPKs, as well as Akt in cultured cardiac myocytes. As shown in Figs. 4A, B, and C, rhCyPA significantly phosphorylated ERK1/2, p38MAPK, and SAPKs, indicating the activation of these kinases. The phosphorylation was led to a maximum level biphasically at 2–5 min and 30 min for ERK1/2 and SAPKs, and at 5–10 min and 30 min for p38MAPK. rhCyPA also significantly phosphorylated

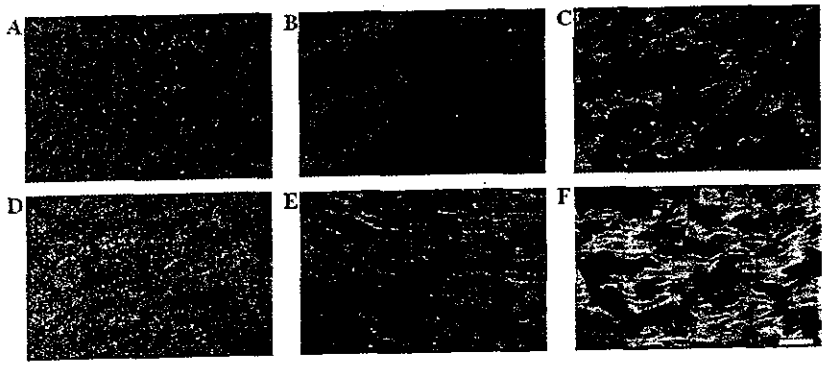

Fig. 3. Immunohistochemical study of ventricular myocardium for CyPA and CD147. Sham-operated myocardium (A), myocardium subjected to ischemia for 30 min (B), and myocardium subjected to ischemia for 30 min followed by reperfusion for 15 min (C) were stained with anti-CyPA antibody. Sham-operated myocardium (D), myocardium subjected to ischemia for 30 min (E), and myocardium subjected to ischemia for 30 min followed by reperfusion for 30 min (F) were stained with anti-CD147 antibody. Bar = 50 μm.

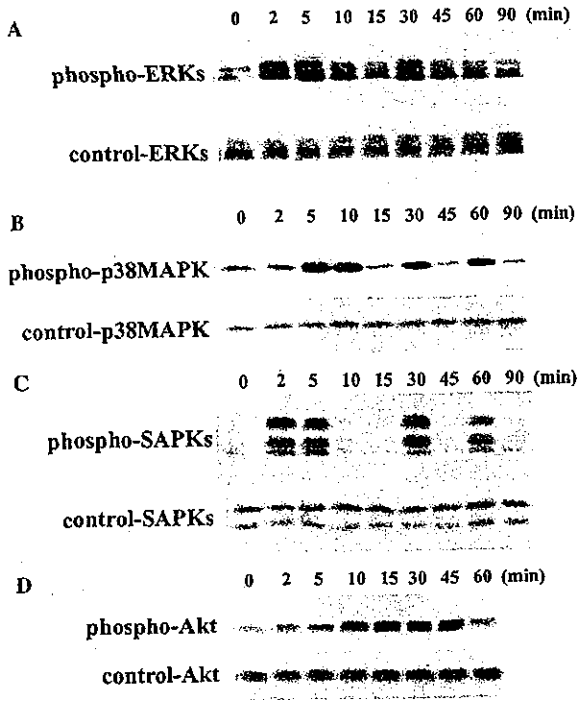

Fig. 4. Recombinant human (rh) CyPA phosphorylates ERK1/2, p38MAPK, SAPKs, and Akt. Serum-starved cardiac myocytes were treated with recombinant human (rh) CyPA (10 nM) for the indicated time periods and lysed in buffer A. The cell lysates were centrifuged and the supernatants were subjected to Western blot analyses using a phospho-specific ERK1/2 (Thr202/Tyr204) (A), p38MAPK (Tyr182) (B), SAPKs (Thr183/Tyr185) (C), or Akt (Ser473) (D) antibody, respectively. Aliquots of the same samples were also subjected to Western blot analyses using a rabbit polyclonal control anti-ERK1/2 (A), p38MAPK (B), SAPK (C), or Akt (D) antibody. The antibody–antigen complexes were developed with chemiluminescence using alkalinephosphatase. The experiments were performed at least in triplicate. The results shown are from one typical experiment.

Akt with a maximum level at 15–30 min. We confirmed that almost equal amounts of ERK1/2, p38MAPK, SAPKs, and Akt proteins were electrophoresed in each reaction by Western blot analyses using control anti-ERK1/2, -p38MAPK, -SAPKs, and -Akt antibodies (phosphorylation-state independent) (Fig. 4).

CyPA increases the expression of Bcl-2 in cultured cardiac myocytes

Because CyPA activates Akt in cardiac myocytes, next, we examined whether CyPA increases anti-apoptotic proteins such as Bcl-2 and Bcl-X_L in cardiac myocytes. As shown in Fig. 5, CyPA significantly increased Bcl-2 with a maximum level at 16 h, whereas CyPA did not significantly change the levels of Bcl-X_L and Bcl-X_S. Western blot analysis using an anti-actin antibody as an internal standard showed that almost equal amounts of samples were electrophoresed in each reaction (Fig. 5).

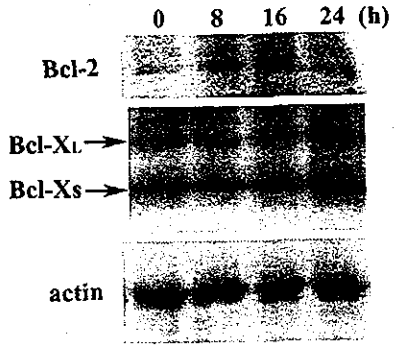

Fig. 5. Effects of recombinant human (rh) CyPA on the expression of Bcl-2 and Bcl-$X_{S/L}$. Serum-starved cardiac myocytes were treated with rhCyPA (50 nM) for the indicated time periods and lysed in buffer A. The cell lysates were centrifuged and the supernatants were subjected to Western blot analyses using an anti-Bcl-2 or -Bcl-X mAb. Aliquots of the same samples were also subjected to Western blot analysis using an anti-actin antibody. The antibody–antigen complexes were developed with chemiluminescence using alkalinephosphatase. The experiments were performed at least in triplicate. The results shown are from one typical experiment.

Discussion

In the present study, we have showed that CyPA was one of the proteins secreted from cultured rat cardiac myocytes in response to hypoxia/reoxygenation and that hypoxia/reoxygenation induced the expression of CyPA and its cell surface receptor CD147 [8] on cardiac myocytes. This strongly suggests that secreted CyPA interacts with CD147 on cardiac myocytes in an autocrine fashion and plays a role in activating intracellular signaling which mediates cardiac response to hypoxia/reoxygenation. We also showed that rhCyPA activated MAPK family kinases and Akt, and significantly increased Bcl-2 in cardiac myocytes, suggesting a protective role for CyPA against oxidative stress-induced apoptosis.

CyPA is an immunophilin family protein known to exist intracellularly and is distributed ubiquitously. CyPA is known to be an enzyme with peptidyl–prolyl *cis–trans* isomerase activity and acts as a molecular chaperone in protein folding [9,10]. In fact, CyPA has been shown to bind with cyclosporine A or is incorporated into human immunodeficiency virus type 1 (HIV-1) particles, and plays an essential role in immunosuppressive effect of cyclosporine A as well as HIV-1 infection [11–13]. In addition to the intracellular function, CyPA has also been shown to be secreted by cells in response to various stimuli and play important roles in chemotaxis of neutrophils, monocytes, and eosinophils as well as in protecting host cells from external stresses [14–16]. Jin et al. [16] reported that CyPA was secreted by vascular smooth muscle cells (VSMCs) in response to oxidative stress induced by LY83583, an O_2^- generator, and that secreted CyPA-mediated ERK activation in VSMCs, increased DNA synthesis, and

inhibited nitric oxide-induced apoptosis in VSMCs. The authors also demonstrated that the expression of CyPA was markedly increased in the balloon-injured vascular lesion, suggesting that CyPA acts as an oxidative stress-responsive growth and survival factor for VSMCs. It has been shown that mammalian cells quickly respond and adapt to external stresses such as mechanical load, metabolic changes, and hypoxia/reoxygenation, by expressing a number of various genes, which may have protective or injurious effects on the cells. In particular, cardiac myocytes express various genes coding for growth factors, cytokines, cell-adhesion molecules, and so on, in response to ischemia/reperfusion to adapt to these stresses or lead to further cell damage known as reperfusion injury. Moreover, evidence has accumulated that cardiac myocytes secrete various growth factors such as angiotensin II, transforming growth factor-β1, endothelin-1, atrial natriuretic peptide, and adrenomedullin, which in turn mediate cellular response to external stresses in an autocrine fashion [17–21]. Kitta et al. [22] reported that hepatocyte growth factor protected cardiac myocytes against apoptosis induced by oxidative stresses such as daunorubicin, serum deprivation, and hydrogen peroxide. In the present study, we have demonstrated for the first time that cardiac myocytes secreted CyPA in response to hypoxia/reoxygenation and that secreted CyPA played a role in activating intracellular signaling through CD147, which was upregulated on cardiac myocytes by hypoxia/reoxygenation. Upregulation of CyPA and CD147 on cardiac myocytes was also confirmed by ischemia/reperfusion in vivo, suggesting that the similar mechanism was involved in cardiac response to ischemia/reperfusion in vivo. Although at least several growth factors may be involved in the cardiac response to oxidative stresses, our data strongly suggest that CyPA plays a role in the protection of cardiac myocytes against oxidative stress-induced apoptosis through this autocrine mechanism.

Acknowledgments

This work was supported by a grant for scientific research from the Ministry of Education, Culture, Sports, Science and Technology, Japan. We thank Mr. S. Kawano, Mr. T. Shino, and Ms. M. Otsuki for their excellent technical assistance.

References

[1] Y. Seko, K. Tobe, K. Ueki, T. Kadowaki, Y. Yazaki, Hypoxia and hypoxia/reoxygenation activate Raf-1, mitogen-activated protein (MAP) kinase kinase, MAP kinases, and S6 kinase in cultured rat cardiac myocytes, Circ. Res. 78 (1996) 82–90.

[2] Y. Seko, K. Tobe, N. Takahashi, Y. Kaburagi, T. Kadowaki, Y. Yazaki, Hypoxia and hypoxia/reoxygenation activate src family tyrosine kinases and $p21^{ras}$ in cultured rat cardiac myocytes, Biochem. Biophys. Res. Commun. 226 (1996) 530–535.

[3] Y. Seko, N. Takahashi, K. Tobe, T. Kadowaki, Y. Yazaki, Hypoxia and hypoxia/reoxygenation activate $p65^{PAK}$, p38 mitogen-activated protein kinase (MAPK), and stress-activated protein kinase (SAPK) in cultured rat cardiac myocytes, Biochem. Biophys. Res. Commun. 239 (1997) 840–844.

[4] R. Mineki, H. Taka, T. Fujimura, M. Kikkawa, N. Shindo, K. Murayama, In situ alkylation with acrylamide for identification of cysteinyl residues in proteins during one- and two-dimensional sodium dodecyl sulphate–polyacrylamide gel electrophoresis, Proteomics 2 (2002) 1672–1681.

[5] H. Selye, E. Bajusz, S. Grasso, P. Mendell, Simple techniques for the surgical occlusion of coronary vessels in the rat, Angiology 11 (1960) 398–407.

[6] Y. Yazaki, H. Tsuchimochi, M. Kuro-o, M. Kurabayashi, M. Isobe, S. Ueda, R. Nagai, F. Takaku, Distribution of myosin isozymes in human atrial and ventricular myocardium: comparison in normal and overloaded heart, Eur. Heart J. 5 (Suppl. F) (1984) 103–110.

[7] Y. Seko, N. Takahashi, M. Azuma, H. Yagita, K. Okumura, Y. Yazaki, Effects of in vivo administration of anti-B7-1/B7-2 monoclonal antibodies on murine acute myocarditis caused by coxsackievirus B3, Circ. Res. 82 (1998) 613–618.

[8] V. Yurchenko, G. Zybarth, M. O'Connor, W.W. Dai, G. Franchin, T. Hao, H. Guo, H.-C. Hung, B. Toole, P. Gallay, B. Sherry, M. Bukrinsky, Active site residues of cyclophilin A are crucial for its signaling activity via CD147, J. Biol. Chem. 277 (2002) 22959–22965.

[9] A. Galat, Peptidylproline *cis–trans*-isomerases: immunophilins, Eur. J. Biochem. 216 (1993) 689–707.

[10] S.F. Gothel, M.A. Marahiel, Peptidyl-prolyl *cis–trans* isomerases, a superfamily of ubiquitous folding catalysts, Cell Mol. Life Sci. 55 (1999) 423–436.

[11] J. Liu, FK506 and cyclosporine, molecular probes for studying intracellular signal transduction, Immunol. Today 14 (1993) 290–295.

[12] D.A. Fruman, S.J. Burakoff, B.E. Bierer, Immunophilins in protein folding and immunosuppression, FASEB J. 8 (1994) 391–400.

[13] J. Luban, K.L. Bossolt, E.K. Franke, G.V. Kalpana, S.P. Goff, Human immunodeficiency virus type 1 Gag protein binds to cyclophilins A and B, Cell 73 (1993) 1067–1078.

[14] B. Sherry, N. Yarlett, A. Strupp, A. Cerami, Identification of cyclophilin as a proinflammatory secretory product of lipopolysaccharide-activated macrophages, Proc. Natl. Acad. Sci. USA 89 (1992) 3511–3515.

[15] Q. Xu, M.C. Leiva, S.A. Fischkoff, R.E. Handschumacher, C.R. Lyttle, Leukocyte chemotactic activity of cyclophilin, J. Biol. Chem. 267 (1992) 11968–11971.

[16] Z.-G. Jin, M.G. Melaragno, D.-F. Liao, C. Yan, J. Haendeler, Y.-A. Suh, J.D. Lambeth, B.C. Berk, Cyclophilin A is a secreted growth factor induced by oxidative stress, Circ. Res. 87 (2000) 789–796.

[17] J. Sadoshima, Y. Xu, H.S. Slayter, S. Izumo, Autocrine release of angiotensin II mediates stretch-induced hypertrophy of cardiac myocytes in vitro, Cell 75 (1993) 977–984.

[18] N. Takahashi, A. Calderone, N.J. Izzo Jr., T.M. Maki, J.D. Marsh, W.S. Colucci, Hypertrophic stimuli induce transforming growth factor-beta 1 expression in rat ventricular myocytes, J. Clin. Invest. 94 (1994) 1470–1476.

[19] Y. Bezie, L. Mesnard, D. Longrois, F. Samson, C. Perret, J.J. Mercadier, S. Laurent, Interactions between endothelin-1 and atrial natriuretic peptide influence cultured chick cardiac myocyte contractility, Eur. J. Pharmacol. 311 (1996) 241–248.

[20] T. Horio, T. Nishikimi, F. Yoshihara, H. Matsuo, S. Takishita, K. Kangawa, Inhibitory regulation of hypertrophy by endogenous atrial natriuretic peptide in cultured cardiac myocytes, Hypertension 35 (2000) 19–24.

[21] F. Yoshihara, T. Horio, T. Nishikimi, H. Matsuo, S. Kangawa, Possible involvement of oxidative stress in hypoxia-induced adrenomedullin secretion in cultured rat cardiomyocytes, Eur. J. Pharmacol. 436 (2002) 1–6.

[22] K. Kitta, R.M. Day, T. Ikeda, Y.J. Suzuki, Hepatocyte growth factor protects cardiac myocytes against oxidative stress-induced apoptosis, Free Radic. Biol. Med. 31 (2001) 902–910.

Membrane-Associated IL-1 Contributes to Chronic Synovitis and Cartilage Destruction in Human IL-1α Transgenic Mice

Yasuo Niki,[1,2*‡] Harumoto Yamada,[†] Toshiyuki Kikuchi,[‡] Yoshiaki Toyama,[*] Hideo Matsumoto,[*] Kyosuke Fujikawa,[‡] and Norihiro Tada[§]

IL-1 molecules are encoded by two distinct genes, IL-1α and IL-1β. Both isoforms possess essentially identical activities and potencies, *whereas IL-1α, in contrast to IL-1β,* is known to act as a membrane-associated IL-1 (MA-IL-1) and plays an important role in a variety of inflammatory situations. The transgenic (Tg) mouse line (Tg1706), which was generated in our laboratory, overexpresses human IL-1α (hIL-1α) and exhibits a severe arthritic phenotype characterized by autonomous synovial proliferation with subsequent cartilage destruction. Because the transgene encoded Lys[64] to Ala[271] of the hIL-1α amino acid sequence, Tg mice may overproduce MA-IL-1 as well as soluble IL-1α. The present study investigated whether MA-IL-1 contributes to synovial proliferation and cartilage destruction in the development of arthritis. Flow cytometric analysis revealed that both macrophage-like and fibroblast-like synoviocytes constitutively produce MA-IL-1. D10 cell proliferation assay revealed MA-IL-1 bioactivity of paraformaldehyde-fixed synoviocytes and the further induction of endogenous mouse MA-IL-1 via autocrine mechanisms. MA-IL-1 expressed on synoviocytes triggered synoviocyte self-proliferation through cell-to-cell (i.e., juxtacrine) interactions and also promoted proteoglycan release from the cartilage matrix in chondrocyte monolayer culture. Interestingly, the severity of arthritis was significantly correlated with MA-IL-1 activity rather than with soluble IL-1α activity or concentration of serum hIL-1α. Moreover, when the Tg1706 line was compared with the Tg101 line, which selectively overexpresses the 17-kDa mature hIL-1α, the severity of arthritis was significantly higher in the Tg1706 line than in the Tg101 line. These results suggest that MA-IL-1 contributes to synoviocyte self-proliferation and subsequent cartilage destruction in inflammatory joint disease such as rheumatoid arthritis. *The Journal of Immunology,* 2004, 172: 577–584.

Rheumatoid arthritis (RA)[3] is characterized by a permanently proliferative synovium, leading to the formation of hyperplastic synovial tissue (pannus) that invades both cartilage and bone. Human IL-1α (hIL-1α) transgenic (Tg) mice overexpressing hIL-1α exhibit macrophage- and neutrophil-dominant arthritis characterized by marked synovial proliferation and progressive cartilage destruction, resembling RA with a progressive phenotype. Histopathological analysis of synovial joints from hIL-1α Tg mice has demonstrated that proliferative synovium directly invades the cartilage, ultimately destroying both cartilage and underlying bone (1). As IL-1 is known to play a pivotal role in the pathogenesis of RA, analysis of IL-1-mediated synovial proliferation and subsequent invasion of the cartilage may elucidate the mechanisms of joint destruction and suggest new therapies for RA.

IL-1 molecules are encoded by two distinct genes, IL-1α and IL-1β. Both genes initially produce precursor polypeptides with a predicted M_r of 31 kDa. IL-1α precursor is fully biologically active and acts as a membrane-associated IL-1 (MA-IL-1), whereas IL-1β precursor displays no biological activity until it has been processed to form the 17-kDa mature form (2, 3). Unlike other secreted proteins, IL-1α precursor lacks a hydrophobic leader sequence (4) and is never found in organelles involved in the classical secretory pathway. The processing and release of IL-1α demonstrate atypical regulation through a number of post-translational modifications (5–7), and the exact processes vary between different cell types (8–10). Our detailed analysis of hIL-1α Tg mice revealed that among various cell types, synoviocytes are the predominant cells producing both precursor and processed forms of hIL-1α despite the use of ubiquitous CAG promoter. This preferential distribution of hIL-1α in synoviocytes seems at least partially due to the extended retention of MA-IL-1 in these cells (1).

In certain situations, IL-1α reportedly acts preferentially as MA-IL-1 (11), which was first described as IL-1 bioactivity within paraformaldehyde (PFA)-fixed macrophage or purified macrophage membranes (12). The presence of IL-1α has subsequently been demonstrated on the surface of various cell types (13–19). A wide spectrum of biological properties has also been reported, including induction of autonomous proliferation in vascular smooth muscle cells (20), T cell activation during Ag presentation (21), up-regulation of monocyte/macrophage-mediated tumor cytotoxicity (22), and stimulation of osteoclast formation (23), where cell-to-cell (i.e., juxtacrine) interactions play a key role in these actions.

The hIL-1α Tg mouse line established in our laboratory was designed to integrate a 660-bp *Hin*dIII/*Hin*cII restriction fragment of hIL-1α cDNA coding Lys[64] to Ala[271] of the hIL-1α amino acid sequence in an attempt to overproduce both pro and mature forms of IL-1α. As the transgene includes a nuclear localization sequence (aa 79–86) that has been shown to be important for IL-1α association with the plasma membrane (24), MA-IL-1 is expected to express in Tg mice and play an important role in the development

*Department of Orthopedic Surgery, Keio University, Tokyo, Japan; †Department of Orthopedic Surgery, Fujita Health University, Aichi, Japan; ‡Department of Orthopedic Surgery, National Defense Medical College, Saitama, Japan; and §Atopy Research Center, Juntendo University School of Medicine, Tokyo, Japan

Received for publication April 11, 2003. Accepted for publication October 24, 2003.

The costs of publication of this article were defrayed in part by the payment of page charges. This article must therefore be hereby marked *advertisement* in accordance with 18 U.S.C. Section 1734 solely to indicate this fact.

[1] Current address: Department of Orthopedic Surgery, Tokyo Women's Medical University, 10-22 Kawada-cho, Shinjuku-ku, Tokyo 162-0054, Japan.

[2] Address correspondence and reprint requests to Dr. Yasuo Niki, Department of Orthopedic Surgery, Keio University, 35 Shinanomachi, Shinjuku-ku, Tokyo 160-8582, Japan. E-mail address: y.niki@lib.bekkoame.ne.jp

[3] Abbreviations used in this paper: RA, rheumatoid arthritis; hIL-1α, human IL-1α; LMMA, L-N^G-monomethyl arginine; MA-IL-1, membrane-associated IL-1; mIL-1α, mouse IL-1α; PFA, paraformaldehyde; PG, proteoglycan; Tg, transgenic.

0022-1767/04/$02.00

of joint destruction. The present study investigated whether biologically active hIL-1α derived from the transgene appears on the surface of synoviocytes, and whether MA-IL-1 contributes to synovial proliferation and cartilage destruction in the development of arthritis in hIL-1α Tg mice. MA-IL-1 was found to be expressed on the surface of synoviocytes from Tg mice and triggered synoviocyte self-proliferation and cartilage destruction in vitro. Interestingly, the activity of MA-IL-1, but not soluble IL-1, in synoviocytes displayed correlations with both macroscopic and histological severity of arthritis in Tg mice. These results suggest that blocking the activities of both membrane-associated and soluble IL-1 may be required to effectively neutralize the pathogenic potential of this cytokine in inflammatory arthropathy such as RA.

Materials and Methods

Generation of Tg mice

The generation of hIL-1α Tg mice has been described previously (1). A 660-bp *Hin*dIII/*Hin*cII restriction fragment of hIL-1α cDNA (Immunex, Seattle, WA) coding Lys^{64} to Ala^{271} of the hIL-1α amino acid sequence was inserted into the *Eco*RI site of the third exon of the rabbit β-globin gene in the expression plasmid, pBsCAG-2. pBsCAG-2 possesses CAG containing the first intron of the chicken β-actin gene and a portion of the rabbit β-globin gene. The resulting construct was excised and microinjected into pronuclei of fertilized one-cell eggs from B6×B6C3F$_1$ mice. The established Tg mouse line (designated Tg1706) was backcrossed with C3H/HeJ mice for six to eight generations and used in all experiments. The Tg101 line, which was designed to integrate 420 bp of mature hIL-1α cDNA coding Ser^{113} to Ala^{271}, was used in a histological examination, and the macroscopic and histological scores were compared with those of Tg1706 (Fig. 1).

Cell culture

Synovial specimens obtained from knee joints of 6- to 8-wk-old Tg mice were treated using 120 U/ml *Streptomyces sp.* C-51 collagenase (Sanko Junyaku, Tokyo, Japan) at 37°C for 30 min. Dispersed synovial cells were allowed to adhere to dishes in DMEM (Life Technologies, Gaithersburg, MD) containing 10% FBS (Life Technologies), 100 U/ml penicillin, and 100 μg/ml streptomycin (Life Technologies). Fifth-passage cells were used in all experiments.

Macroscopic and histological assessment of arthritis

Clinical symptoms of arthritis in all four limbs were macroscopically evaluated according to a visual scoring system. Arthritic joints were graded on a scale of 0–4: 0 = no change, 0.5 = swelling and erythema of 1 digit, 1 = swelling and erythema of ≥2 digits, 2 = mild swelling and erythema of the limb, 3 = gross swelling and erythema of the limb, and 4 = gross deformity and inability to use the limb. Scoring was performed in a blinded fashion by two observers, and the macroscopic score for each mouse comprised the sum of scores for all four limbs, for a maximum score of 16. In histological evaluations, ankle and knee joints were dissected and fixed in formalin. Sagittal sections (6 μm) were prepared and stained using H&E. Using the method described by van den Berg et al. (25), synovial infiltration and cartilage destruction were scored on four semiserial sections of each specimen spaced 10 sections apart. Neutrophil infiltration was graded on a scale of 0–3, according to the number of neutrophils in synovial tissue. Cartilage destruction was also graded on a scale of 0–3: 0 = no change, 1 = dead chondrocytes (empty lacunae) or focal loss of cartilage, 2 = loss of 25–50% of cartilage, and 3 = complete loss of cartilage. Scoring was performed again in a blinded fashion by two observers, and histological scores for each mouse comprised the sum of scores for two hind limbs, for a maximum score of 24.

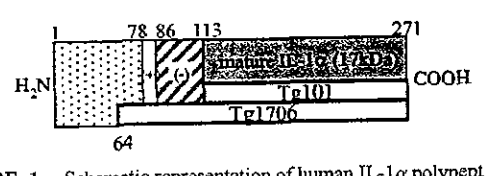

FIGURE 1. Schematic representation of human IL-1α polypeptide. The transgenes of Tg1706 and Tg101 coded Lys^{64} to Ala^{271} and Ser^{113} to Ala^{271} of human IL-1α amino acid sequence, respectively: ▩, N-terminal conserved region (Met^{1}-Gly^{78}); □ (+), multiple basic region known as nuclear localization sequence (Lys^{79}-Arg^{86}); ▨ (−), negatively charged region (Leu^{86}-Arg^{112}); ■, mature 17-kDa IL-1α (Ser^{113}-Ala^{271}).

Flow cytometric analysis of MA-IL-1 synthesis

MA-IL-1 synthesis by synoviocytes was analyzed using flow cytometry. Briefly, adherent synoviocytes (1–5 × 10^5 cells/test) were harvested and placed in ice-cold 5 mM EDTA and 1% BSA in Ca^{2+}/Mg^{2+}-free PBS at 37°C for 15 min. In accordance with the method described by Bailly et al. (26), either with or without 144 h of fixation in 1% (v/v) PFA at room temperature, synoviocytes were incubated for 15 min with unlabeled anti-CD16/32 (2.4G2; BD PharMingen, San Diego, CA) to block nonspecific binding to FcRII/III. Cells were then stained using PE-labeled anti-hIL-1α mAb (BD Immunocytometry Systems, San Jose, CA). In two-color analysis of freshly isolated synoviocytes, cells were further stained with biotinylated anti-F4/80 Ab (Cedarlane Laboratories, Hornby, Ontario, Canada), then incubated with cytochrome-conjugated streptavidin (BD Immunocytometry Systems). PE-conjugated mouse IgG (BD PharMingen) was used as an isotype-matched control to exclude the possibility of nonspecific binding. Stained cells were then analyzed using FACScan (BD Biosciences, Mountain View, CA). In some experiments cells were treated with 0.01 μg/ml trypsin before PFA fixation, then subjected to flow cytometry.

Immunoprecipitation of synoviocyte membrane fraction

Cultured synoviocytes were maintained in methionine/cysteine-free medium (Life Technologies) for 2 h, then medium was replaced with freshly prepared appropriate deficient medium containing 40 μCi/ml [^{35}S]methionine/cysteine (Amersham Pharmacia Biotech, Little Chalfont, U.K.) for 6 h, and washed three times using ice-cold PBS. The synoviocyte membrane fraction was prepared as previously described (27). Briefly, cultured synoviocytes harvested with ice-cold 5 mM EDTA in PBS were suspended at a concentration of 5 × 10^6 cells/ml in ice-cold homogenization buffer (20 mM Tris-HCl (pH 7.4), 10 mM NaCl, 0.1 mM $MgCl_2$, 0.1 mM PMSF, and 0.5 mg/ml DNase I), followed by sonication three times for 15 s each time. Homogenate was centrifuged at 95,000 × *g* for 1 h over 41% (w/v) sucrose solution. The [^{35}S]methionine/cysteine-labeled membrane fraction was recovered from the interface and treated with lysis buffer (150 mM NaCl, 10 mM Tris-HCl (pH 7.5), 1% deoxycholate, 1% Triton X-100, 0.1% SDS, 10 mM EDTA, and 2 mM PMSF). This isolated membrane fraction was concentrated 5- to 10-fold in a Centricon Centrifugal Concentrator (Millipore, Bedford, MA), then subjected to immunoprecipitation with anti-hIL-1α polyclonal Ab (Endogen, Woburn, MA) using an ImmunoPure Protein A IgG Orientation Kit (Pierce, Rockford, IL). In some experiments, 20 μg of unlabeled recombinant hIL-1α (Genzyme, Cambridge, MA) was added during immunoprecipitation. Labeled proteins in immunoprecipitates and ^{14}C-methylated protein M_r marker (Amersham Pharmacia Biotech) were prepared for electrophoresis on 12.5% SDS-polyacrylamide gels, fixed, and treated with ENLIGHTNING (PerkinElmer, Boston, MA). Gels were dried and exposed to film at −80°C for autoradiography.

Bioassay for MA-IL-1 and soluble IL-1

MA-IL-1 bioactivity in synoviocytes was quantitated by PFA fixation of cells, as described by Bailly et al. (26). Briefly, synoviocytes were inoculated at 5 × 10^4 cells/well on 96-well, flat-bottom tissue culture plates (BD Biosciences, Franklin Park, NJ). After culturing for 24 h, cells were fixed with 1% PFA in PBS (pH 7.4) at room temperature for 144 h, washed three times, and incubated in 100 μl of medium for 24 h. IL-1-sensitive mouse T cell clone D10.G4.1 (D10) cells (provided by Dr. Tadakuma, National Defense Medical College) were propagated as described previously (28), then used as an indicator for the presence of IL-1. In the synoviocyte proliferation assay, Tg mouse-derived synoviocytes were used as indicators for IL-1. Indicator cells were distributed to wells at a concentration of 4 × 10^4 cells/well containing fixed synoviocytes in a total volume of 200 μl of medium supplemented with 1 μg/ml Con A (Sigma-Aldrich, St. Louis, MO). In assays for soluble IL-1, indicator cells were similarly distributed to wells in medium containing 25% (v/v) final concentration of samples, instead of fixed cells. The incorporation of [^{3}H]thymidine into indicator cells was measured during the final 4 h of the 48-h culture. In some experiments neutralizing Abs against human IL-1α (20 μg/ml; Endogen) and/or mouse IL-1α (20 μg/ml; R&D Systems, Minneapolis, MN) were added to cultures during assays. Normal rabbit or goat IgGs (R&D Systems) were used as isotype-matched controls for anti-human or anti-mouse IL-1α neutralizing Ab, respectively. The mitogenic activity of 100 pg/ml

recombinant human IL-1α (Endogen) was determined to provide a reference for the magnitude of the effects of MA-IL-1 expressed on fixed synoviocytes.

Effect of cell culture inserts on MA-IL-1 activity

Synoviocytes were inoculated at 1.5×10^5 cells/well on 24-well, flat-bottom tissue culture plates (BD Biosciences). After 24 h of culture, cells were fixed with 1% PFA in PBS (pH 7.4) at room temperature for 144 h. Live synoviocytes were added to wells as indicator cells at 1.5×10^5 cells/well in a total volume of 500 μl, either directly or into the top compartment of the Cell Culture Insert (BD Biosciences). Incorporation of [^{3}H]thymidine into live synoviocytes was measured during the final 24 h of the 48-h culture. For blockade of IL-1, neutralizing Abs against hIL-1α (20 μg/ml; Endogen) and/or mouse IL-1α (20 μg/ml; R&D Systems) were added to cultures during assays.

Analysis of kinetics for synthesis of MA-IL-1 and soluble IL-1

Synoviocytes were inoculated at 1.5×10^5 cells/well on 24-well, flat-bottom plates (BD Biosciences) in a total volume of 500 μl and incubated for 24, 48, 72, or 96 h, and culture supernatants were collected before fixation in 1% PFA for 144 h. In MA-IL-1 assays, 1.5×10^5 D10 cells were added to PFA-fixed synoviocytes. In soluble IL-1 assays, 1.5×10^5 D10 cells were incubated with a 25% (v/v) final concentration of culture supernatants from the corresponding time points. Incorporation of [^{3}H]thymidine into D10 cells was measured during the final 4 h of the 48-h culture.

Proteoglycan release assay

Articular chondrocytes were obtained from glenohumeral joints of young Japanese White rabbits. Freshly isolated chondrocytes were seeded at 1×10^5 cells/ml in a 24-well, flat-bottom plate (BD Biosciences). After 1 wk of culture, confluent cells were incubated for 24 h in 500 μl of fresh medium containing [^{35}S]sulfate (Amersham Pharmacia Biotech) at 5 μCi/ml and washed four times with cold fresh medium. Radiolabeled cells were further incubated for 48 h in the presence or the absence of detergent-insoluble membrane fraction isolated from synoviocytes. In some wells, labeled cells were incubated with membrane fraction isolated from trypsin-treated synoviocytes or with 100 μM L-N^G-monomethyl arginine (LMMA; Wako Pure Chemical Industries, Osaka, Japan), an NO synthase inhibitor. The amount of ^{35}S-labeled proteoglycan (PG) in cell and matrix layer and in supernatant was determined as previously described (29). Briefly, ^{35}S-labeled cells and supernatants were separated. A total of 25 μl of supernatant was solubilized using 75 μl of 1.33 M guanidine HCl with 0.5% Triton X-100. Twenty-five microliters of ^{35}S-labeled cell and matrix layer was solubilized for 4 h at 4°C with 4 M guanidine HCl and 0.05 M sodium acetate, pH 6.0, containing protease inhibitors, followed by dilution with 75 μl of dilution buffer containing 0.5% Triton X-100. Next, 100 μl of each sample was prepared in a 96-well MultiScreen filtration plate assembly (Millipore), and 150 μl of 0.2% Alcian Blue was added to the well. Well contents were then filtered through the Millipore Durapore membrane (0.45-μm pore size). Unincorporated [^{35}S]sulfate was removed by three passages of vacuum filtration with wash buffer through the membrane. The membrane disc in each well was punched out and applied to the scintillation counter. All samples were analyzed in triplicate. PG release into supernatant was calculated according to the following equation: % PG release = [([^{35}S]PG in supernatant)/([^{35}S]PG in cell and matrix + [^{35}S]PG in supernatant)] × 100%.

Statistical analysis

Results were expressed as the mean ± SEM. Statistical comparisons were performed using nonparametric Mann-Whitney *U* tests. Correlation analysis was performed using StatView-J 5.0 statistical software (SAS Institute, Cary, NC). A value of $p < 0.05$ was considered statistically significant.

Results

Flow cytometric analysis of MA-IL-1

Two-color flow cytometric analysis of transgene-derived MA-IL-1 revealed that freshly isolated synoviocytes consisted of ~80% F4/80$^+$ synovial macrophages and 20% F4/80$^-$ synovial fibroblasts (Fig. 2*A*, *left panel*). In histogram analysis, ~78% of F4/80$^+$ cells and 70% of F4/80$^-$ cells expressed MA-IL-1 on their cell surface (Fig. 2*A*, *right panel*). As hIL-1α Tg mice constitutively express transgene under the control of CAG promoter, both types of synoviocytes constitutively produced hIL-1α. The fact that membrane permeabilization was not required for staining synoviocytes with PE-labeled hIL-1α Ab ensured cell surface distribution of hIL-1α (Fig. 2*B*, *left panel*). Identical staining patterns were observed in PFA-fixed synoviocytes (Fig. 2*B*, *middle panel*). Furthermore, this membrane-localized IL-1 in synoviocytes was removed with mild trypsin treatment (Fig. 2*B*, *right panel*), as reported by others (9, 30). This indicates that MA-IL-1 was substantially anchored in the membrane, with tryptic cleavage sites exposed on the cellular surface.

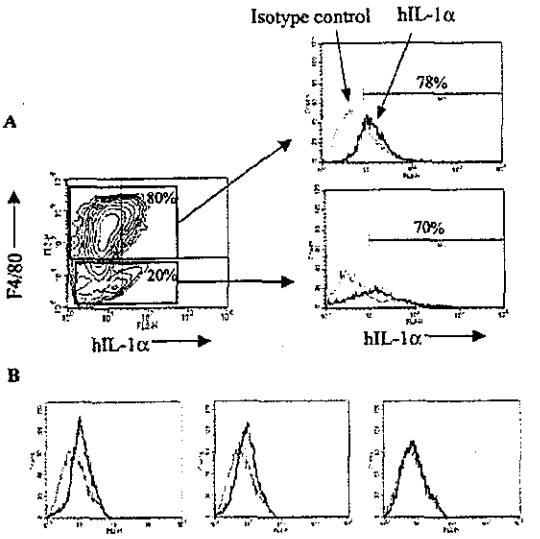

FIGURE 2. Flow cytometric analysis of transgene-derived MA-IL-1 on the surface of synoviocytes. *A*, Freshly isolated synoviocytes from 8-wk-old Tg mice were stained with PE-labeled anti-hIL-1α Ab in conjunction with biotinylated anti-F4/80 Ab to identify synovial macrophages (*right panel*). The levels of MA-IL-1 after gating on F4/80$^+$ cells or F4/80$^-$ cells are shown in histograms. The percentage of cells expressing MA-IL-1 is indicated (*right panel*). The results are representative of three different experiments. *B*, MA-IL-1 expression in fifth-passage synoviocytes (purity of synovial fibroblasts, >95%). Histograms show effects of PFA-fixation and mild trypsin treatment on the staining pattern of cell surface hIL-1α. MA-IL-1 can be detected on the surface of synoviocytes in both the presence (*middle panel*) and absence (*left panel*) of PFA fixation. MA-IL-1 exposed on the surface of synoviocytes was removed by mild trypsin treatment (*right panel*). Gray lines show the background with isotype-matched control Abs. Results are representative of three different experiments.

Immunoprecipitation of MA-IL-1

To further confirm membrane localization of transgene-derived hIL-1α, a membrane fraction was isolated from synoviocytes, and immunoprecipitation was performed using specific Abs. The results clearly indicated that transgene-derived hIL-1α within the membrane fraction included a 25-kDa protein, slightly heavier than the 23-kDa primary translation product of the transgene (Fig. 3). In fact, culture supernatants and cell lysates of synoviocytes displayed both 23- and 25-kDa hIL-1α proteins (1). However, only the 25-kDa protein was detected in the membrane fraction. This preferential distribution of 25-kDa hIL-1α implies the promotion of post-translational modifications probably related to membrane localization of hIL-1α, such as phosphorylation (5), mannosylation (6), and myristolation (7). To examine whether this band was the truth, competition analysis was performed by adding excess unlabeled recombinant hIL-1α (~2.0 μg) during immunoprecipitation. As expected, recombinant hIL-1α completely prevented the immunoprecipitation of labeled hIL-1α with specific Ab, whereas neither recombinant hIL-1β nor mouse IL-1α (mIL-1α) demonstrated any